

https://doi.org/10.1038/s42004-024-01306-z

# A new electrolyte for molten carbonate decarbonization

Check for updates

Gad Licht<sup>1</sup>, Kyle Hofstetter<sup>2</sup>, Xirui Wang<sup>2</sup> & Stuart Licht <sup>1,3</sup> ⊠

The molten  $\text{Li}_2\text{CO}_3$  transformation of  $\text{CO}_2$  to oxygen and graphene nanocarbons (GNCs), such as carbon nanotubes, is a large scale process of  $\text{CO}_2$  removal to mitigate climate change. Sustainability benefits include the stability and storage of the products, and the GNC product value is an incentive for carbon removal. However, high  $\text{Li}_2\text{CO}_3$  cost and its competitive use as the primary raw material for EV batteries are obstacles. Common alternative alkali or alkali earth carbonates are ineffective substitutes due to impure GNC products or high energy limitations. A new decarbonization chemistry utilizing a majority of  $\text{SrCO}_3$  is investigated.  $\text{SrCO}_3$  is much more abundant, and an order of magnitude less expensive, than  $\text{Li}_2\text{CO}_3$ . The equivalent affinities of  $\text{SrCO}_3$  and  $\text{Li}_2\text{CO}_3$  for absorbing and releasing  $\text{CO}_2$  are demonstrated to be comparable, and are unlike all the other alkali and alkali earth carbonates. The temperature domain in which the  $\text{CO}_2$  transformation to GNCs can be effective is <800 °C. Although the solidus temperature of  $\text{SrCO}_3$  is 1494 °C, it is remarkably soluble in  $\text{Li}_2\text{CO}_3$  at temperatures less than 800 °C, and the electrolysis energy is low. High purity CNTs are synthesized from  $\text{CO}_2$  respectively in  $\text{SrCO}_3$  based electrolytes containing 30% or less  $\text{Li}_2\text{CO}_3$ .

In 2015, a decarbonization technique was introduced for the transition metal nucleated transformation of CO<sub>2</sub> to nanoallotropes of carbon. This single-step decarbonization process in molten carbonates electrochemically splits CO<sub>2</sub> into carbon and oxygen via the C2CNT (carbon dioxide to carbon nanomaterial technology) process. Catalyzed by transition metals, such as iron, nickel, and chromium, carbon growth is tuned by variations in the composition of the electrolysis electrode, current density, and temperature, forming high-purity graphene nanocarbons (GNCs), such as carbon nanofibers and nanotubes<sup>1–5</sup>. Sustainability benefits include the stability and storage of the GNC products. Their graphene structure is stable for effective sequestration, and the GNC high product value is an incentive for carbon removal. The current value of GNCs is due to the high strength, conductivity electronic, medical and catalytic properties of graphene allotropes and their open market value of approximately a million \$US/tonne<sup>1</sup>.

Alternatively, commercial carbon nanotubes are generally produced by chemical vapor deposition  $(\text{CVD})^{6-10}$ , often with a large carbon footprint due to chemical fuel precursors and increased energy consumption<sup>11</sup>. The CVD synthesis of carbon nanotubes includes organometallics. A recent study presented the formation of carbon nanofibers from  $\text{CO}_2$  in a multistep process<sup>12</sup>. First,  $\text{CO}_2$  and water were electrolyzed to form syngas, and then, the syngas was used as a reactant to produce carbon nanofibers by CVD. In particular, the study stated that a disadvantage of C2CNT, rather than CVD, is that C2CNT competes for limited lithium carbonate supplies used in the

battery industry (for example, lithium carbonate is a principal precursor in the fabrication of Li-ion batteries in EVs).

The physical and chemical systems for carbon nanotube (CNT) synthesis using conventional chemical vapor deposition (CVD) differ significantly from those of the new C2CNT synthesis. CVD is a chemical process that occurs at a gas/solid interface, typically using various organometallic compounds as reactants, and is associated with a high carbon footprint. In contrast, C2CNT is an electrochemical process that transforms  $CO_2$  into CNTs through molten electrolysis, operating at a liquid/solid interface with a carbon-negative footprint.

The C2CNT process benefits from a molten carbonate electrolyte that provides a higher density of reactive carbon sites—specifically, tetravalent carbon available for reduction at the molten carbonate/cathode interface—compared to the lower density of carbon available as a gas in CVD. While CVD may apply an electric field to the substrate during CNT growth, C2CNT consistently involves a strong electric field that rapidly decreases through the double layer adjacent to the cathode. One of the key advantages of C2CNT is that its production cost is predominantly influenced by the cost of electrons (electricity), leading to substantial cost reductions compared to conventional CVD methods.

The C2CNT electrodes were scaled up by one thousand-fold from the  $5~{\rm cm}^2$  electrodes used in the 2015 design and assembled in electrolysis modules, which collectively comprise 1000 tons of  ${\rm CO}_2$  decarbonization. Panel A of Fig. 1 shows a photograph of the scaled-up brass cathode extracted after

<sup>1</sup>C2CNT LLC, A4 188 Triple Diamond Blvd, Venice, FL, 34275, USA. <sup>2</sup>Carbon Corp, 1035 26 St NE, Calgary, AB, T2A 6K8, Canada. <sup>3</sup>Department of Chemistry, George Washington University, Washington, DC, 20052, USA. ⊠e-mail: slicht@gwu.edu

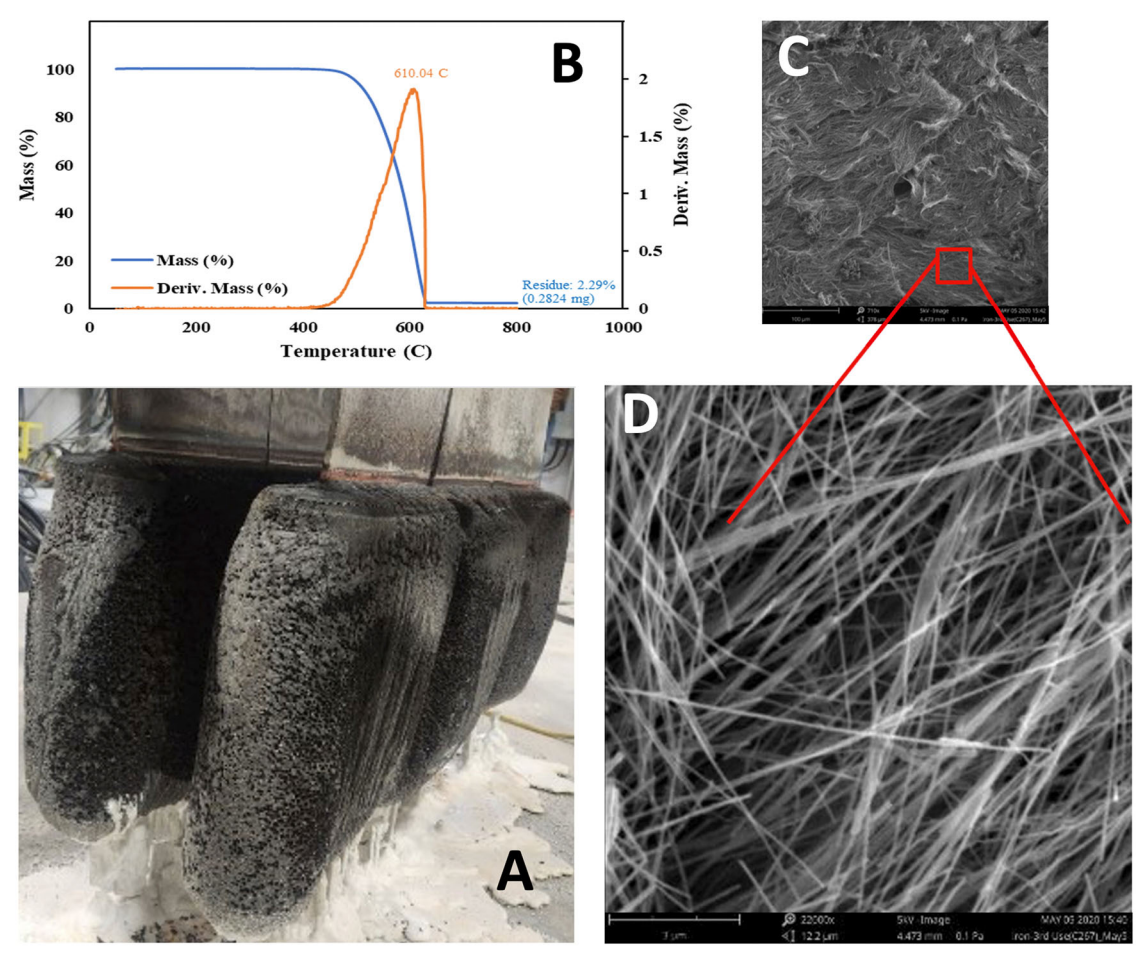


Fig. 1 | Large-scale C2CNT electrolysis. A Photo of an extracted cathode after current density  $J = 0.2 \text{ A/cm}^2$  electrolysis of  $CO_2$  in a pure 750 °C  $Li_2CO_3$  electrolyte. B TGA, C, D SEM images of the washed carbon nanotube product. The SEM images are at magnifications of (B) 710× and (C) 2250×.

electrolysis of  $\rm CO_2$  for 16 h in a lithium carbonate electrolyte. After electrolysis, the product is subsequently pressed and/or washed to remove and recover the remaining electrolyte from the product. SEM images of the washed products were obtained at magnifications of 710× and 2250×, and the images show that the CNTs had a purity >>90%. Panel B of the figure shows the TGA analysis and a product purity >97%. Furthermore, TGA exhibited an inflection temperature of  $\rm T_{infl}$  = 610 °C, which is a combustion point consistent with an oxidation-resistant nanographene structure and is unlike an alternative common amorphous carbon that oxidizes at several hundred degrees lower temperature.

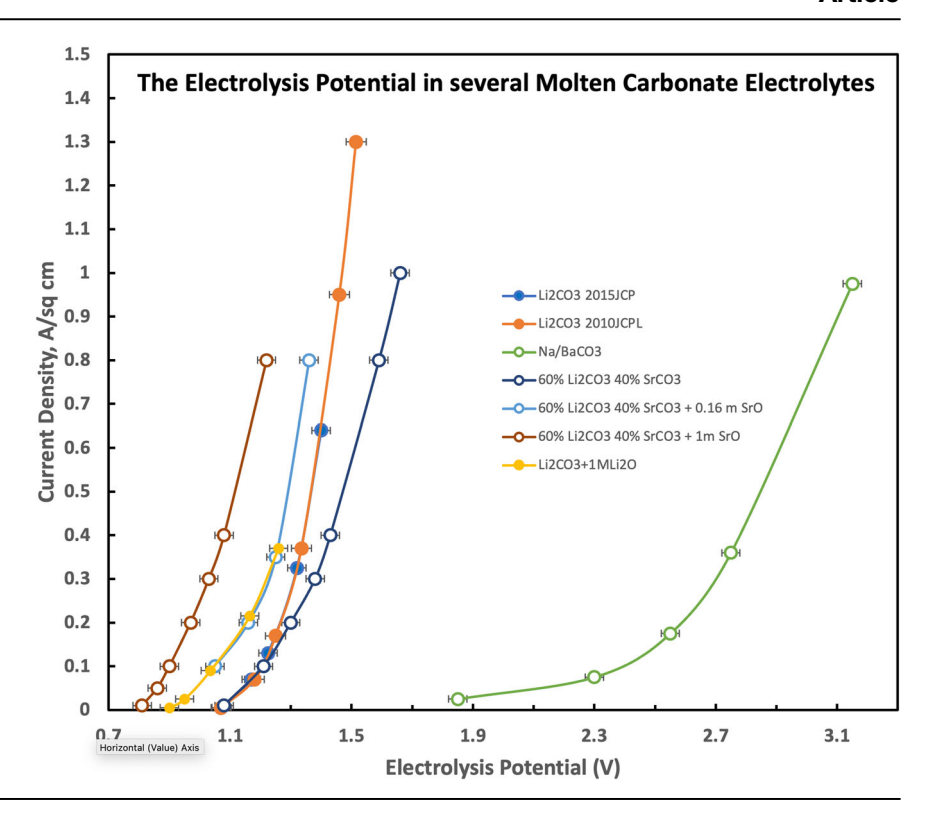
Subsequent to this electrolysis, fivefold larger cathodes are regularly used. The average GNC purity ranged from 90 to 98%, depending on the pure Li<sub>2</sub>CO<sub>3</sub> electrolysis conditions and post-electrolysis press extraction and/or polishing washing. In accordance with the electrolytic splitting of CO<sub>2</sub>: CO<sub>2</sub> -> C<sub>GNC</sub> + O<sub>2</sub>, 1 tonne of GNC is synthesized via the C2CNT process, which removes 3.7 tonnes of CO<sub>2</sub> from the atmosphere or flue gas. GNCs have found applications in materials such as medicine, polymers, batteries, cement, and textiles  $^{13-26}$ .

Variations in the electrolysis electrode composition, current density, oxide addition, and electrolysis temperature tune C2CNT electrolysis to form long<sup>27,28</sup>, tangled<sup>1,29</sup>, thin-walled<sup>30</sup>, helical<sup>31</sup>, magnetic<sup>32</sup>, nanobamboo, branched, and anopearl carbon nanotube, and conical nanofiber morphologies<sup>4,5</sup>. The addition of boron, sulfur, or nitrate salts produces doped carbon nanotubes<sup>27,28,33</sup>. Further variations in the lithium carbonate electrolysis conditions facilitate the formation of alternative, pure carbon nanoallotropes, including solid or hollow carbon nanoallotropes<sup>4,34</sup>, graphene nanoscaffolds<sup>35</sup>, graphene nanoplatelets, or graphene<sup>36</sup>.

 $\rm Li_2CO_3$  is expensive, and this is in part due to the competitive demand for  $\rm Li_2CO_3$ , particularly for use in the preparation of Li-ion batteries for the growing electronic vehicle (EV) market. Global  $\rm Li_2CO_3$  prices for 2022 to 2024 vacillate in the range of \$10,000–75,000 per tonne. These elevated prices present a cost constraint to the alternative use of  $\rm Li_2CO_3$  as a molten electrolyte in the transformation, by electrolytic splitting, of  $\rm CO_2$  in  $\rm Li_2CO_3$  to GNCs. This study develops the fundamental chemistry and demonstrates the efficacy of a new, substantially more cost-effective electrolyte for molten carbonate decomposition.

We had explored the growth of CNTs in alternative molten carbonate electrolytes, often without success. The pure salts Li<sub>2</sub>CO<sub>3</sub>, Na<sub>2</sub>CO<sub>3</sub>, and K<sub>2</sub>CO<sub>3</sub> have melting points at 723 °C, 851 °C and 891 °C, respectively. Eutectic ternary mixes of Li<sub>2</sub>CO<sub>3</sub>, Na<sub>2</sub>CO<sub>3</sub>, and K<sub>2</sub>CO<sub>3</sub> have been well characterized as molten carbonate electrolytes and do not produce significant amounts of CNT products<sup>37</sup>. Potassium carbonate, as a component of a binary lithium carbonate electrolyte, tends to disrupt the electrocatalytic, highly stable oxide layer that forms on the electrolysis anode and results in corrosion of the anode<sup>38</sup>. Increasing K<sub>2</sub>CO<sub>3</sub> also inhibits transition metal nucleation at higher concentrations<sup>39</sup>. The synthesized carbon nanotubes are increasingly defect-ridden at contents of 20% K<sub>2</sub>CO<sub>3</sub> or higher<sup>39</sup>. At 50 wt% K<sub>2</sub>CO<sub>3</sub> in Li<sub>2</sub>CO<sub>3</sub>, metallic potassium, rather than carbon, forms, and the product ignites when exposed to humid air, while no CNTs are formed from a Na<sub>2</sub>CO<sub>3</sub>-K<sub>2</sub>CO<sub>3</sub> electrolyte<sup>37,38</sup>. Upon electrolysis, a binary mixture of sodium and Li<sub>2</sub>CO<sub>3</sub> produces CNTs up to 20 wt% Na<sub>2</sub>CO<sub>3</sub>, but beyond that, the product is increasingly deformed<sup>39</sup>. Interestingly, at a lower electrolysis temperature of 670 °C, rather than 770 °C, 50 wt% sodium carbonate and 50 wt% Li<sub>2</sub>CO<sub>3</sub> form another GNC, other

Fig. 2 | Carbonate electrolysis potential measured in several molten carbonates. The electrolytes investigated included pure lithium carbonate or pure lithium carbonate with 1.0 m Li<sub>2</sub>O, an equal mixture of sodium and barium carbonate, a mixture of 40 wt% strontium carbonate with 60 wt% Li<sub>2</sub>CO<sub>3</sub>, or a mixture of the latter with either 0.16 or 1.0 m SrO and are reproducible to 30 mV. Electrolysis Potentials of Li<sub>2</sub>CO<sub>3</sub> with or without Li<sub>2</sub>O was obtained from our measurements in refs. 2,56, and Na/BaCO<sub>3</sub> was obtained from ref. 2. The additional strontium-containing electrolyte electrolysis potentials were measured in this study.



than CNTs, which we have termed carbon nanoscaffolds<sup>35</sup>. Furthermore, the addition of Na<sub>2</sub>CO<sub>3</sub> to Li<sub>2</sub>CO<sub>3</sub> considerably increases the electrolysis potential<sup>2</sup>.

Magnesium carbonate decomposes to magnesium oxide and CO<sub>2</sub> above 350 °C, while calcium carbonate decomposition to lime above 840 °C is the basis of cement production. Barium carbonate melts at 811 °C and has a eutectic morphology with lithium carbonate at 609 °C<sup>40</sup>. The addition of magnesium carbonate to lithium carbonate suppresses CNT formation, resulting in a product with a honeycomb morphology with only a small amount of thin-walled CNTs33. CNTs are grown in lithium carbonate containing up to approximately 20 wt% calcium and barium carbonate  $^{33,37,41,42}$ .  $CO_2$  electrolysis in a mixed calcium carbonate/lithium carbonate electrolyte proceeds differently than that in other mixed lithium carbonate electrolytes. In lithium or lithium/barium electrolytes, lithium or barium oxide is highly soluble, whereas calcium oxide is soluble only to 0.2 m CaO in Li<sub>2</sub>CO<sub>3</sub><sup>40,41</sup>. Hence, during electrolysis, rather than reacting with CO2, the oxide precipitates out as calcium oxide, while calcium carbonate is consumed rather than CO<sub>2</sub> splitting. The addition of magnesium, calcium, or barium carbonate to lithium carbonate was observed to cause an unfavorable increase in the electrolysis potential<sup>2,33</sup>.

Despite its high solidus temperature of 1494 °C, in the present study, strontium carbonate was shown to be unusually soluble in lithium carbonate at temperatures less than 800 °C. Strontium carbonate is the only carbonate with a similar thermodynamic affinity for CO<sub>2</sub> to that of lithium carbonate, and as with lithium carbonate, it supports low-energy decarbonization to form useful CNT products. Concentrated strontium carbonate electrolytes are demonstrated here to form high-purity CNT products, and as opposed to lithium carbonate are a cost-effective electrolyte for molten carbonate electrolysis. To date, there have been no successful decarbonization chemistries deployed to meaningfully mitigate planetary climate change. Climate change is an existential threat to the planet, and to the majority of the species on the planet including humankind. The new strontium decarbonization chemistry presented in this study has the potential to be the first such decarbonization chemistry. The never before described strontium chemistry is analyzed in depth from a thermodynamic and practical standpoint.

#### Results and discussion

#### Electrolysis and electrolysis potentials in molten carbonate

An Illustration of the C2CNT process, detailed SEM, TEM, HAADF, RXRD and Raman of the synthesized carbon nanotubes, as well as examples of the range of graphene nanocarbon allotropes synthesized from CO<sub>2</sub> by molten carbonate electrolysis are included in the Supplementary Material.

The electrochemical reduction of  ${\rm CO_3}^{2-}$  in molten carbonate is a 4e process:

$$CO_3^{2-}$$
 (molten)  $\rightarrow$  C(nanomaterial) +  $O_2$ (gas) +  $O^{2-}$ (dissolved) (1)

The  $\rm CO_2$  added to the electrolyte chemically reacts with the oxide formed through Eq. 1 to renew  $\rm CO_3^{2-}$  following Eq. 2:

$$CO_2(gas) + O^{2-}(dissolved) \rightarrow CO_3^{2-}(molten)$$
 (2)

Combining Eqs. 1 and 2 yields a net decarbonization reaction:

$$CO_2(gas) \rightarrow C(nanomaterial) + O_2(gas)$$
 (3)

We previously synthesized CNTs by electrolysis in 50/50 wt% Na/BaCO<sub>3</sub>, albeit by forming CNTs at a lower purity than that of pure Li<sub>2</sub>CO<sub>3</sub> <sup>43</sup>. However, this synthesis requires severalfold more electrolysis power to drive the reaction. Figure 2 compares the molten carbonate electrolysis potential of several electrolytes. Compared to 1 V, which drives CNT formation in lithium carbonate, the Na/BaCO<sub>3</sub> potential results in a two- to threefold greater voltage and inordinately high energy consumption to drive a decarbonization process.

## The unexpectedly high solubility of strontium salts in molten $\text{Li}_2\text{CO}_3$

Interestingly, there is little, or no, information available on the melting point of the binary mixture of pure  $\text{Li}_2\text{CO}_3/\text{(mp 723 °C)}$  with  $\text{SrCO}_3$  (which is solid to 1494 °C). One study revealed that  $\text{SrCO}_3$  fully decomposes to SrO as the temperature increases from 875 °C to 1035 °C<sup>44</sup>. It is discovered that  $\text{SrCO}_3$  is highly soluble in molten lithium carbonate at temperatures

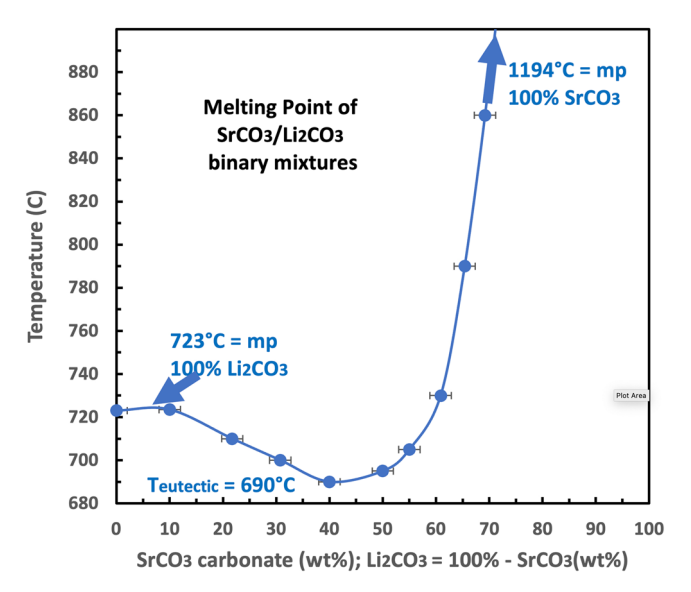


Fig. 3 | The melting point and high SrCO<sub>3</sub> solubility of binary mixtures of SrCO<sub>3</sub> and Li<sub>2</sub>CO<sub>3</sub>. Measured solubilities are reproducible to <2%.

<800 °C and that the inexpensive SrCO<sub>3</sub> salt can replace a major portion of the expensive lithium carbonate salt as an electrolyte for decarbonization and CNT growth. We find that strontium oxide, SrO, which can facilitate the rapid reactive dissolution of CO<sub>2</sub>, is also highly soluble (at ~25 wt% in Li<sub>2</sub>CO<sub>3</sub> at 750 °C) when measured here using 99% SrO. The efficacy of these salts as electrolytes for molten electrolysis at temperatures below 800 °C is important because above these temperatures, CO<sub>2</sub> increasingly electrolytically splits to gaseous carbon monoxide rather than to the desired solid-phase GNC products, and by 950 °C, the product is entirely CO rather than solid GNCs<sup>43</sup>.

The measured melting points of binary mixtures of  $SrCO_3$  and  $Li_2CO_3$  as a function of temperature are presented in Fig. 3. The figure shows that the solubility of 99.4% purity  $SrCO_3$  in  $Li_2CO_3$  (99.8%, Green Chemical Co.) reaches 65 wt% in the regular  $CO_2$  splitting temperature domain (T < 800 °C). The binary mixture exhibited a minimum (eutectic point) melting point at 690 °C occurring at a composition of 40 wt%  $SrCO_3$ . It is likely that ternary materials composed of Li- $SrCO_3$  plus other salt mixes will exhibit lower eutectic temperatures. A lower 98.6% purity  $SrCO_3$ , containing minor ternary mix components (0.8%  $SrCO_3$  and 0.2 wt%  $SrCO_3$ ), exhibited a slightly lower eutectic temperature of 880 °C at 40 wt% composition in the same 60 wt%  $SrCO_3$ .

SrCO<sub>3</sub> is available at a more stable global price of approximately \$1,040/ton, a cost that is 1 to 2 orders of magnitude less than that of Li<sub>2</sub>CO<sub>3</sub><sup>45,46</sup>. Strontium is the tenth most abundant metal in the earth's core, while lithium is twenty-fourth most abundant<sup>47</sup>. Strontium carbonate is widely mined and refined to from strontium sulfate or carbonate. Previously, strontium carbonate was used in glass compositions for television and cathode ray devices but is not used in today's flat screens. Today, strontium is used in pyrotechnics and in various applications, including ceramics, ferrite magnets, superconductors, biomaterials, chemical sensors, and catalysts 48-50. It is also used to protect certain magnesium alloys against corrosion<sup>51,52</sup> and in specialized cement compositions<sup>53–55</sup>. However, SrCO<sub>3</sub> is solid at 1494 °C, which is too high for CO<sub>2</sub> electrolysis to solid carbon products. We have demonstrated that temperatures below 800 °C are suitable for CO<sub>2</sub> molten carbonate electrolysis. At higher temperatures, another product, carbon monoxide, increasingly forms, and the product is pure carbon monoxide at 950 °C<sup>56</sup>. Carbon monoxide is not preferred as a decomposition product. Its main use is as an oxidant, and in that process, it returns CO<sub>2</sub> to the atmosphere. Alternatively, GNCs retain the high geologic stability of mineral graphite to sequester CO2.

## The overlapping affinity of strontium and lithium carbonate for binding and releasing CO<sub>2</sub>

 ${\rm CO}_2$  is a critical decarbonization component in molten carbonate electrolytic splitting and the transformation of  ${\rm CO}_2$  to GNCs. In particular, the affinity of lithium carbon for  ${\rm CO}_2$  provides a balance both facilitating rapid  ${\rm CO}_2$  intake into the molten salt and providing an enriched carbon electrolytic media. The enriched carbon electrolytic media facilitates the electrochemical reduction of tetravalent carbon to carbon. The enriched media has an observed the low overpotential to generate high electrolysis rates and also specifically generates GNCs, as observed by the high purity of GNCs, such as CNTs. Here, we calculate the  ${\rm CO}_2$  affinity of SrCO<sub>3</sub> and show that, unlike nonlithium alkali carbonates or other alkali earth carbonates, SrCO<sub>3</sub> exhibits a  ${\rm CO}_2$  affinity equivalent to that of  ${\rm Li}_2{\rm CO}_3$ . The equilibrium, K(MCO<sub>3</sub>), for alkali and alkali earth carbonates to separate into  ${\rm CO}_2$  and oxide, or to form carbonate from them in the reverse reaction, is given by the equilibrium for the decomposition, or in reverse for formation, of a carbonate from  ${\rm CO}_2$  and its oxide:

$$MCO_3 \rightleftharpoons CO_2 + MO$$
  $KMCO_3 = pco_2 a_{MO}/a_{MCO_3}$  (4)

where examples of M are Li2, Na2, K2, Mg, Ca, Ba or Sr.

The equilibrium,  $K_{MCO3}$ , is calculated from the relationship between the equilibrium and free energy, where the gas constant R=8.31 J/mol K:

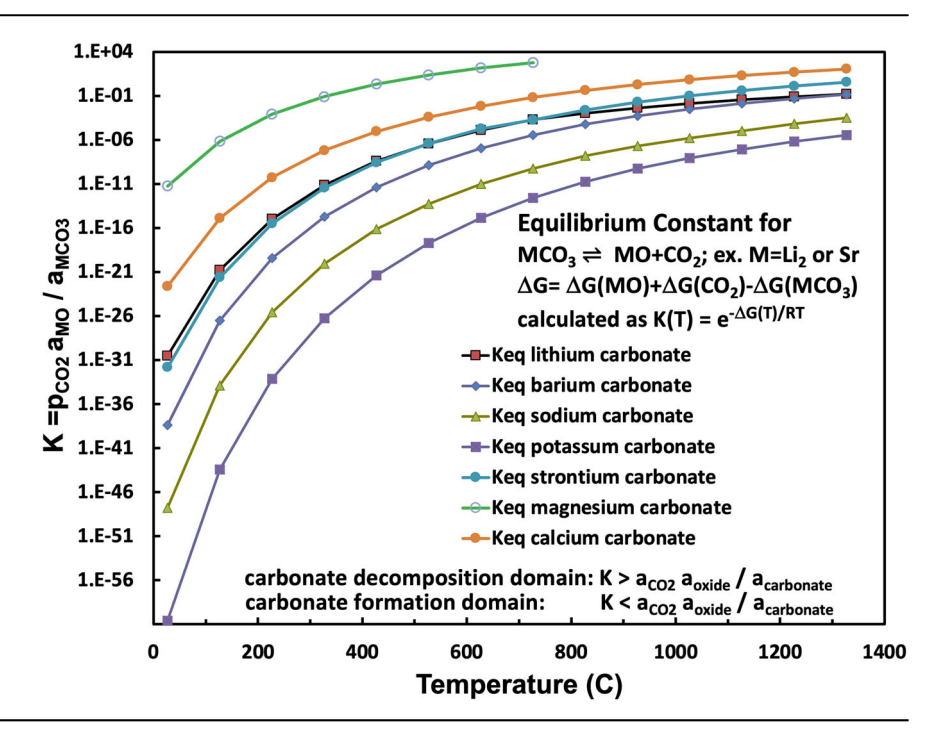
$$\Delta G^{o}MCO_{3} = -RTlnKMCO_{3}; \quad KMCO_{3}\left(T\right) = e^{-\Delta G\left(T\right)/RT} \quad \ (5)$$

 $K_{MCO3}$  is calculated from the thermochemical free energies for a variety of alkali and alkali earth carbonates, their oxides, and  $CO_2$ .

Figure 4 presents a comparison of carbonate equilibrium constants for binding and releasing carbon dioxide by strontium carbonate compared to those for alkali or other alkali earth carbonates. These values are plotted as a function of temperature. Above any given salt equilibrium curve, that is, in the low CO<sub>2</sub> activity domain (a<sub>CO2</sub> a<sub>oxide</sub>/a<sub>carbonate</sub> < K), the salt will spontaneously decompose, while in the high CO<sub>2</sub> activity domain, the salt will spontaneously form from CO<sub>2</sub> and the salt's oxide. Interestingly, as shown in the figure, the strontium carbonate equilibrium is similar to that of lithium carbonate and very different from that of the other carbonate salts. Specifically, the carbonate equilibrium constants for strontium and lithium carbonate are nearly identical in the 400 °C to 800 °C range, in which lithium carbonate binary and trinary salt mixes are molten. We previously observed a high tendency for electrolytic graphene nanocarbon formation in the 600 °C to 800 °C temperature range. At lower temperatures, transition metal nucleation growth of carbon /nanotubes is not observed<sup>37</sup>, and at increasing temperatures above 800 °C, 2-electron reduction to CO, rather than 4-electron reduction to carbon, increasingly dominates. The comparable nature of strontium to lithium carbonate equilibria provides an unusual environmental media conducive to the electrolytic splitting of carbon dioxide and its transformation to graphene nanocarbons.

Isotopic tracking with <sup>13</sup>C was employed to follow the reduction of CO<sub>2</sub> as it is dissolved in molten carbonate and undergoes electrolytic splitting to generate the building blocks of CNTs3. Mechanistically in the 600° to 800°C domain maximizing CNT yield and purity, we hypothesize that the facilitated molten carbonate growth is related to a thermodynamic "Goldilocks" range with an optimal activation barrier for the kinetic binding and reduction of CO2 in accord with Eqs. 2, 3 and 4. More specifically, at 750 °C, in accord with Fig. 4, K<sub>MCO3</sub>, the equilibrium constant for CO<sub>2</sub> release calculated from the Eq. 5 free energies of the carbonate and oxide salts and CO<sub>2</sub>, are 700 and 0.1 respectively for magnesium and calcium carbonate. In these cases, CO<sub>2</sub> is weakly bound. This is consistent with the low temperature of calcination decomposition of these salts. This facile release of CO<sub>2</sub> to the gas phase provides an insufficient source in the molten salt for CO<sub>2</sub> splitting inhibiting CNT growth. Conversely at 750 °C  $K_{MCO3}$  are  $6 \times 10^{-6}$ ,  $1 \times 10^{-9}$ and  $5 \times 10^{-13}$  respectively for barium, sodium and potassium carbonate indicative in each case that CO2 is tightly bound (favoring the left side of Eq. 4) and less available for CO<sub>2</sub> splitting in the 600° to 800 °C range.

Fig. 4 | Equilibrium constant for  $CO_2$  release for a range of alkali and alkali earth carbonates. The equilibrium constants as a function of temperature for strontium, lithium, sodium, potassium, and barium carbonate. The equilibrium constants are calculated from the free energy according to Eq. 5. The free energy is calculated from the metal carbonate, metal oxide, and carbon dioxide enthalpies and entropies<sup>2,69-72</sup>.



As opposed to the too loosely bound  $CO_2$  in magnesium and calcium carbonate, and the too tightly bound  $CO_2$  in barium, sodium, and potassium carbonates, the "Goldilocks"  $CO_2$  carbonate binding for 750 °C  $K_{\rm MCO3}$  is calculated as  $3\times 10^{-4}$  and  $7\times 10^{-4}$  respectively for lithium and strontium carbonate. From the high-quality syntheses from strontium carbonate-based electrolytes which will be presented in the remainder of this study, it may be that the somewhat stronger  $CO_2$  binding by strontium carbonate may be closer to the ideal  $K_{\rm MCO3}$  than that of lithium carbonate.

## The overlapping electrolysis potentials of strontium and lithium carbonate

Figure 2 compares the electrolysis potentials measured in 40 wt% strontium carbonate/60 wt% lithium carbonate electrolytes, both with and without added oxide, and compares these potentials to the electrolysis potentials for pure Li<sub>2</sub>CO<sub>3</sub> with and without oxide and for the Na/BaCO<sub>3</sub> electrolyte. As shown in the figure, the electrolysis potential in pure Li<sub>2</sub>CO<sub>3</sub>, as indicated by the solid orange and dark blue dots, decreases when 1 m of Li<sub>2</sub>O is added to the electrolyte, as indicated by the solid yellow dots. The observed onset potential for CO<sub>2</sub> reduction decreases from 1.08 V in the pure Li<sub>2</sub>CO<sub>3</sub> electrolyte to 0.9 V with 1 m of Li<sub>2</sub>O. As shown in the figure, the onset potential is the same for pure Li<sub>2</sub>O<sub>3</sub> as for the 40%/60% SrCO<sub>3</sub>/Li<sub>2</sub>CO<sub>3</sub> electrolyte. This finding correlates with the similarity discussed above in the equilibrium constants for the two salts in Fig. 3. The 40%/60% SrCO<sub>3</sub>/ Li<sub>2</sub>CO<sub>3</sub> 770 °C electrolysis potentials are presented as hollow dark blue circles. This electrolyte exhibited a moderately higher overpotential at increasing current density than did pure Li<sub>2</sub>CO<sub>3</sub>. Interestingly, the 40%/60% mixed electrolyte is more sensitive to oxide addition when SrO is added than is the pure Li<sub>2</sub>CO<sub>3</sub> electrolyte when Li<sub>2</sub>O is added. As shown in the figure, the addition of only 0.16 m SrO to the mixed electrolyte results in a similar decrease in potential to that in the 1 m Li<sub>2</sub>O Li<sub>2</sub>CO<sub>3</sub> electrolyte. As seen by the brown circles in the figure, the addition of 1 m SrO to the 40%/60% SrCO<sub>3</sub>/Li<sub>2</sub>CO<sub>3</sub> electrolyte further decreases the electrolysis potential to an onset potential of only 0.8 V, and even at higher current densities, the electrolysis potential is lower than that in the Li<sub>2</sub>CO<sub>3</sub> electrolytes.

## Concentrated strontium electrolyses at 0.2 A/cm<sup>2</sup> or 0.6 high A/cm<sup>2</sup> current density

Electrolyzing was performed at 750 °C in lithium media with increasing concentrations of strontium carbonate using a vertical, flat Muntz brass cathode sandwiched between vertical, flat stainless steel cathodes (the

anodes are walls of the carbon pot). Electrolysis was studied as a function of electrolyte composition, electrolysis current density, electrolysis time, number of repeated uses of the electrolyte and carbon pot, and electrolysis electrode size. For electrolytes containing 10, 25, 35, or 45% strontium carbonate at 750 °C, the resultant high-purity CNT product was comparable to that obtained with a pure lithium carbonate electrolyte. Figure 5 shows the TGA and SEM results for the product obtained from electrolysis of 25 wt%  $SrCO_3$  in  $Li_2CO_3$  at a current density of J = 0.2 A/cm<sup>2</sup> for 4 h. As seen via SEM, compared with those of the pure Li<sub>2</sub>CO<sub>3</sub> product, the CNTs are of comparable high (» 90%) purity (Fig. 1), and according to the TGA results, the post-combustion residue is less than 4%, while the TGA inflection point temperature for combustion is 650 °C. EDS along the CNT strands under an SEM revealed 100% elemental carbon, while the SEM bright spots at the CNT tips were iron<sup>5</sup>. In prior studies, we have extensively documented the Raman spectra, TEM results, points of nucleation, EDS and HAADF elemental analysis, and X-ray diffraction data of synthesized GNCs<sup>1-5,27-39</sup>. In this study, we focus instead on the physical chemistry of the solubility, equilibration, and demonstration of the synthesis of high-purity GNCs, such as CNTs and carbon nano-onions, with an unusual series of readily available strontium carbonate electrolytes to ensure their wide availability for large-scale decarbonization.

A comparable CNT product was obtained at an electrolysis current density of 0.2 A/cm² for both less concentrated (10 wt%) and more concentrated (35 wt%) SrCO $_3$  in Li $_2$ CO $_3$  electrolytes, each studied at a current density of J = 0.2 A/cm². Additional electrolysis in the 25 wt% SrCO $_3$  electrolyte was repeated a total of 9 times, reusing the same electrolyte and the same carbon pot and cathode. Electrolysis yielded comparable quality CNT products with no indication of deterioration of the carbon pot, the anode comprising the inner walls of the carbon pot or the cathode.

In addition to a 4-h electrolysis at a current density of  $0.2~A~cm^{-2}$ , electrolyses were also conducted in a 25 wt% SrCO $_3$  electrolyte at a lower current density ( $0.1~A~cm^{-2}$ ) and for a longer electrolysis duration (16~h). Finally, electrolysis at a high current density of  $0.4~A~cm^{-2}$  for four hours was performed in the 35 wt% SrCO $_3$  electrolyte. In both cases, the 0.1~A and 0.4~A electrolyses again produced a comparable quality of carbon nanotubes.

Figure 6 shows the results obtained for a high concentration (45 wt%) of  $SrCO_3$  as an electrolyte for electrolysis in the high-current domain of  $0.6~A~cm^{-2}$ . As seen in TEM (6 A to C) the product remains pure carbon nanotubes graphene walls adjacent to a hollow core. The nucleation metal in

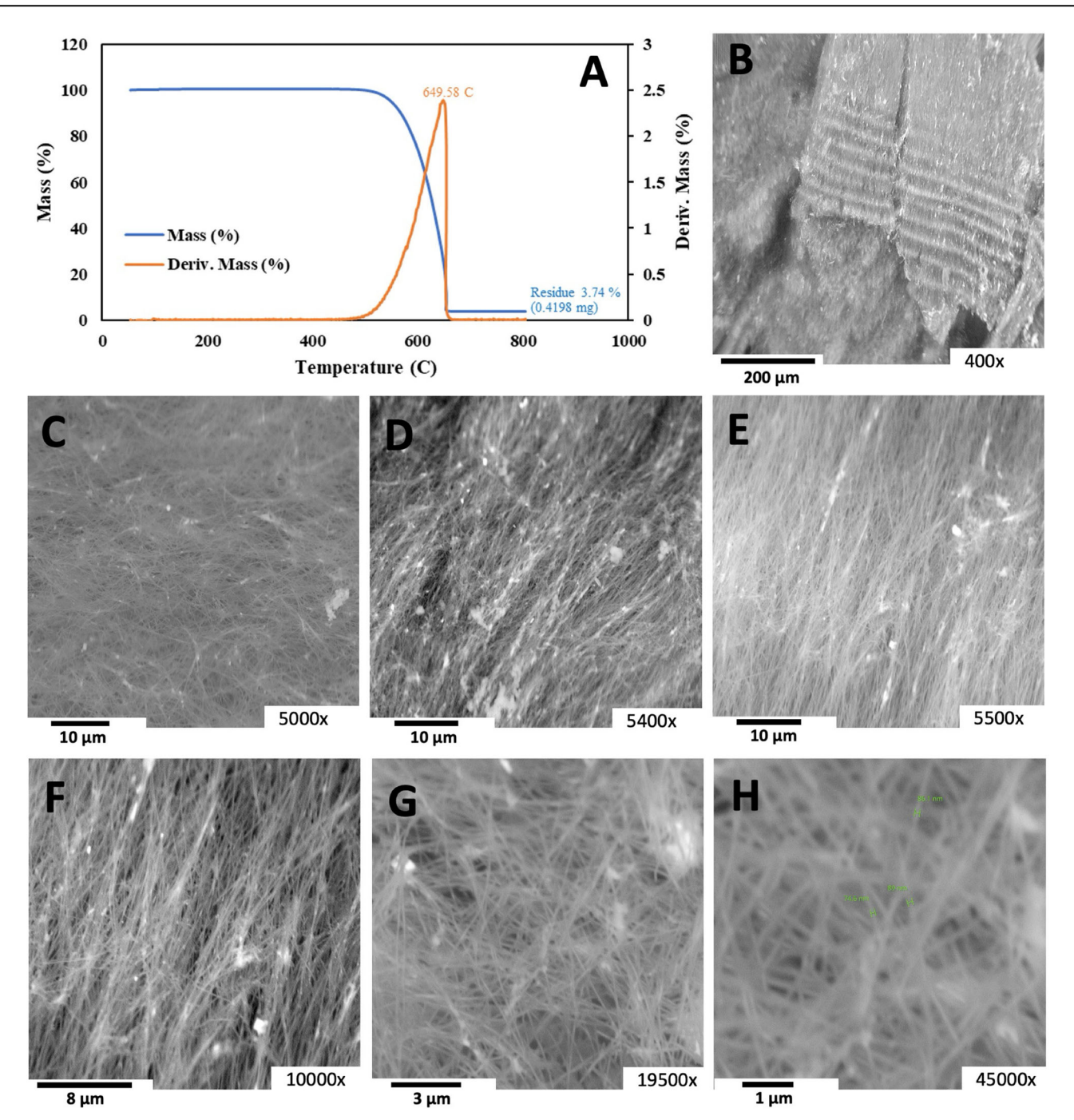


Fig. 5 | TGA and SEM images of the carbon nanotube product of 25 wt% SrCO<sub>3</sub> in a Li<sub>2</sub>CO<sub>3</sub> electrolyte. Four-hour electrolysis was conducted at 750 °C and J = 0.2 A/cm<sup>2</sup> with a stainless steel 304 anode at a 65 cm<sup>2</sup> area brass cathode. A TGA The SEM

magnifications are as follows: B 400×, C 5000×, D 5400×, E 5500×, F 10000×, G 19500×, H 45,000× magnification.

the inner tip of the CNT is seen in 6 A. All of the CNTs exhibit a wall of cylindrical graphene layers next to the hollow portion of the CNT as seen in 6B and 6 C. In 6B, the hollow core and the curving of the cylindrical graphene walls exhibit the typical 0.34 nm separation of graphene layers. Further down the tube, in 6 C are seen the horizontal layered graphene cylinders of the adjacent wall on the other side of the hollow core of the carbon nanotube. We have previously studied the role of the iron, nickel, chromium or other transition metal, individually or in combination, on the formation of various graphene nanocarbon allotropes<sup>4</sup>, or specifically on the carbon nanotube product<sup>1,5,30–33,39</sup>. Initial EDS analysis confirms that iron is the principal nucleating metal for these strontium-based electrolyte carbon nanotubes. A more detailed analysis will be expanded on in a future study.

The  $0.6~{\rm A~cm^{-2}}$  electrolysis domain is pertinent because it provides an industrial high rate of material production. This is the same high current density used in the contemporary high-rate industrial production of aluminum (in which aluminum oxide, rather than carbon dioxide, is electrolyzed) and the current density used in the industrial electrolytic production of magnesium. Electrolysis was conducted at an elevated temperature of 790 °C to enhance mass transport under these higher current density conditions. However, as will be seen in subsequent studies, a lower temperature of 770 °C is also effective under high current density conditions.

As shown in Fig. 6, D through I, SEM at various magnification of the CNT product obtained by high-current density electrolysis in the 45 wt%

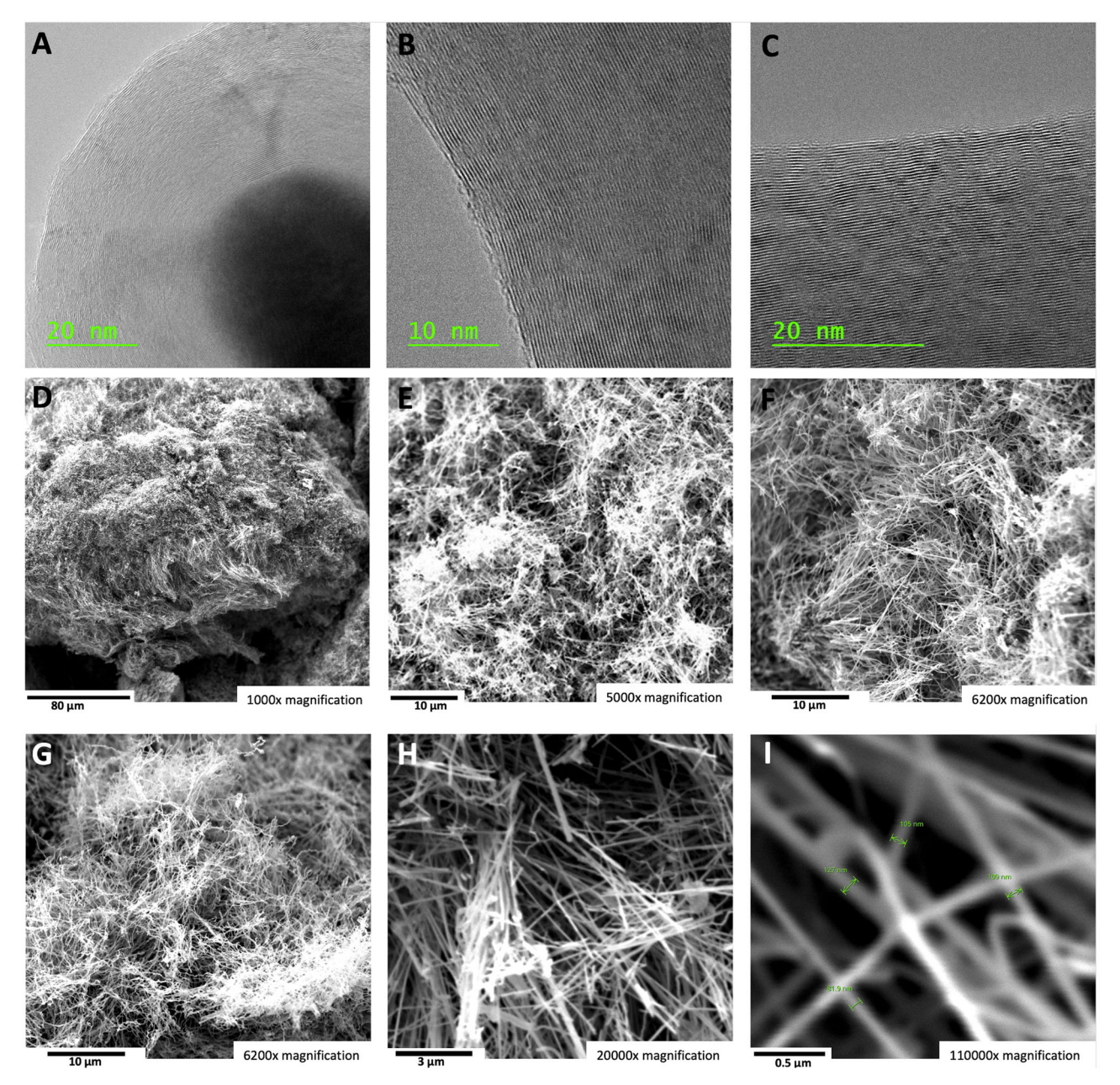


Fig. 6 | The carbon nanotube product of high current electrolysis in a 45 wt%  $SrCO_3$  in a  $Li_2CO_3$  electrolyte. SEM images of the product from 4-h electrolysis conducted at 790 °C and J = 0.6 A/cm² with a stainless steel 304 anode at a 120 cm² area brass cathode. A–C TEM with 20 nm (A & C) and 10 nm (B) scale (3.5 to 7

million  $\times$  magnification) showing the distinctive hemispherical concentric graphene layers surrounding the nucleation catalyst (C) and the concentric graphene adjacent layers above and below the hollow core (B, C). SEM magnification is D 1000 $\times$ , E 5000 $\times$ , F, G 6200 $\times$ , H 20,000 $\times$ , or I 110,000 $\times$  magnification.

SrCO<sub>3</sub> electrolyte yields a comparable quality CNT product to that shown in Figs. 1, 5. We previously found that high current density conditions can induce torsional growth of CNTs<sup>31</sup>, and a minor, but evident, increase in tangling of the carbon nanotubes is observed in the high current density growth product in Fig. 6.

#### Electrolyses with 50 and 60 wt% strontium carbon electrolytes

During the course of the high-solubility domain experiments summarized in Fig. 3, upon stirring with a stainless steel spatula, the highest-solubility domain (65%  $SrCO_3$  in  $Li_2CO_3$ ) electrolytes were more viscous. Hence, initial higher domain, 50%  $SrCO_3$  electrolysis experiments were conducted at higher temperatures and lower than 0.6 A cm<sup>-2</sup> to overcome the anticipated mass transfer limitations. As shown in the Fig. 7 SEM A through F the product of 785 °C electrolysis at a current density of 0.28 A/cm<sup>2</sup> continues to be the high-purity CNTs observed as the product of lower  $SrCO_3$ 

concentration electrolyses. Due to its lower combustion temperature compared to graphene nanocarbon, amorphous carbon is more susceptible to oxidation, burning easily and exhibiting a TGA derivative of mass versus temperature inflection point,  $T_{\rm infb}$  at approximately 300 °C. Alternatively, as seen in Fig. 1, carbon nanotubes possess a high degree of graphitization with typical >600 °C. Similarly, the carbon nanotubes synthesized in the strontium-based electrolytes retain this high degree of graphitization as exemplified for the 50% strontium carbonate electrolyte in Fig. 6G, with measured  $T_{\rm infl}$  = 622 °C.

#### Strontium electrolyte electrolysis at large electrodes

The results shown in Figs. 5–7 were obtained for small or medium-sized Muntz brass cathodes. Specifically, the electrolyses in Figs. 5, 6 were conducted at cathodes with a surface area under 200 cm², while the Fig. 7 electrolysis utilized a cathode with an area of 1600 cm². Strontium electrolyte

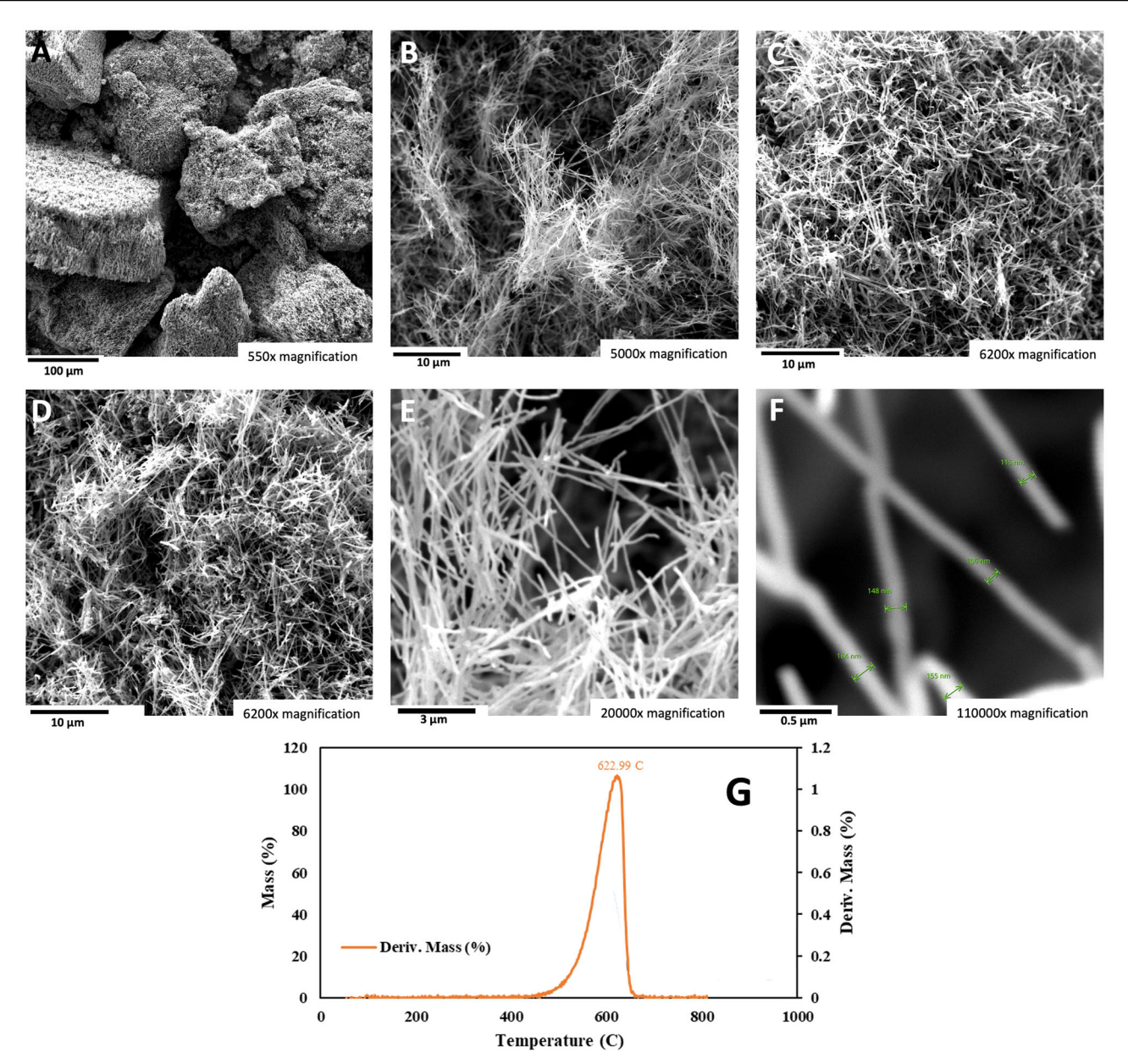


Fig. 7 | The carbon nanotube product of electrolysis in a 50 wt% SrCO<sub>3</sub>/50 wt% Li<sub>2</sub>CO<sub>3</sub> electrolyte. SEM images and TGA of the product from 16-h electrolysis conducted at 785 °C and J = 0.28 A/cm² with a stainless steel 304 anode at a 1600 cm² area brass cathode. The SEM magnifications are A 15500×, B 5000×, C 6200×,

D 6200×, E 20,000×, and F 110,000× magnification. G Differential TGA of the mass loss for the 50% Sr electrolyte product measured with a temperature ramp of 5  $^{\circ}$ C/ minute under air.

electrolysis can be routinely performed with larger cathodes (and at higher current densities) to facilitate large-scale carbon capture.

Figure 8 shows the results for a 770 °C 50% SrCO $_3$  and 50% Li $_2$ CO $_3$  0.6 A/cm $^2$  current density electrolysis at an 11,000 cm $^2$  surface area on a Muntz brass cathode. Panel A of the figure shows the hot Muntz brass cathode subsequent to electrolysis as lifted from the electrolysis chamber below. Panel B shows the same cathode subsequent to cooling. The cathode deposit is approximately 4" thick. SEM characterization of the product of this high surface area, high current density 40% SrCO $_3$  electrolysis is shown in the figure. Once again, a high-purity CNT product is obtained, and as was observed in the other high-current density electrolysis in Fig. 6; an increase in the tangling of the carbon nanotubes is evident in the carbon nanotube product.

Note that the cathode in Fig. 8 is vertically oriented. This considerably decreases the physical plant footprint required for C2CNT decarbonization. Aluminum production has been restricted to horizontal electrodes because

the aluminum product is molten and, during electrolysis, lies on top of the cathode at the bottom of the aluminum pot. Aluminum can also require greater kiln insulation due to the lower pot packing conditions and aluminum production's higher 960 °C pot operating temperature.

## 60 to 64% binary and ternary $SrCO_3$ electrolytes with 35 to 40% $Li_pCO_3$

The success of the 50% SrCO $_3$  electrolysis suggested that lower temperatures were viable for concentrated electrolytes. Therefore, a 60% SrCO $_3$  in 40% Li $_2$ CO $_3$  electrolyte was conducted at 770 °C. Figure 9 summarizes the SEM characterization of the product of the 60% SrCO $_3$  electrolysis. Once again, a high-purity CNT product is attained.

We previously observed that low-level Li<sub>2</sub>O additions can improve the purity of Li<sub>2</sub>CO<sub>3</sub> electrolyses<sup>32</sup>. Oxides can induce twisting of carbon nanotubes due to an increase in sp<sup>3</sup> defects<sup>1,29,31</sup> and, in one case, branched rather than discrete CNT forms<sup>4</sup>, and in this case the observed high

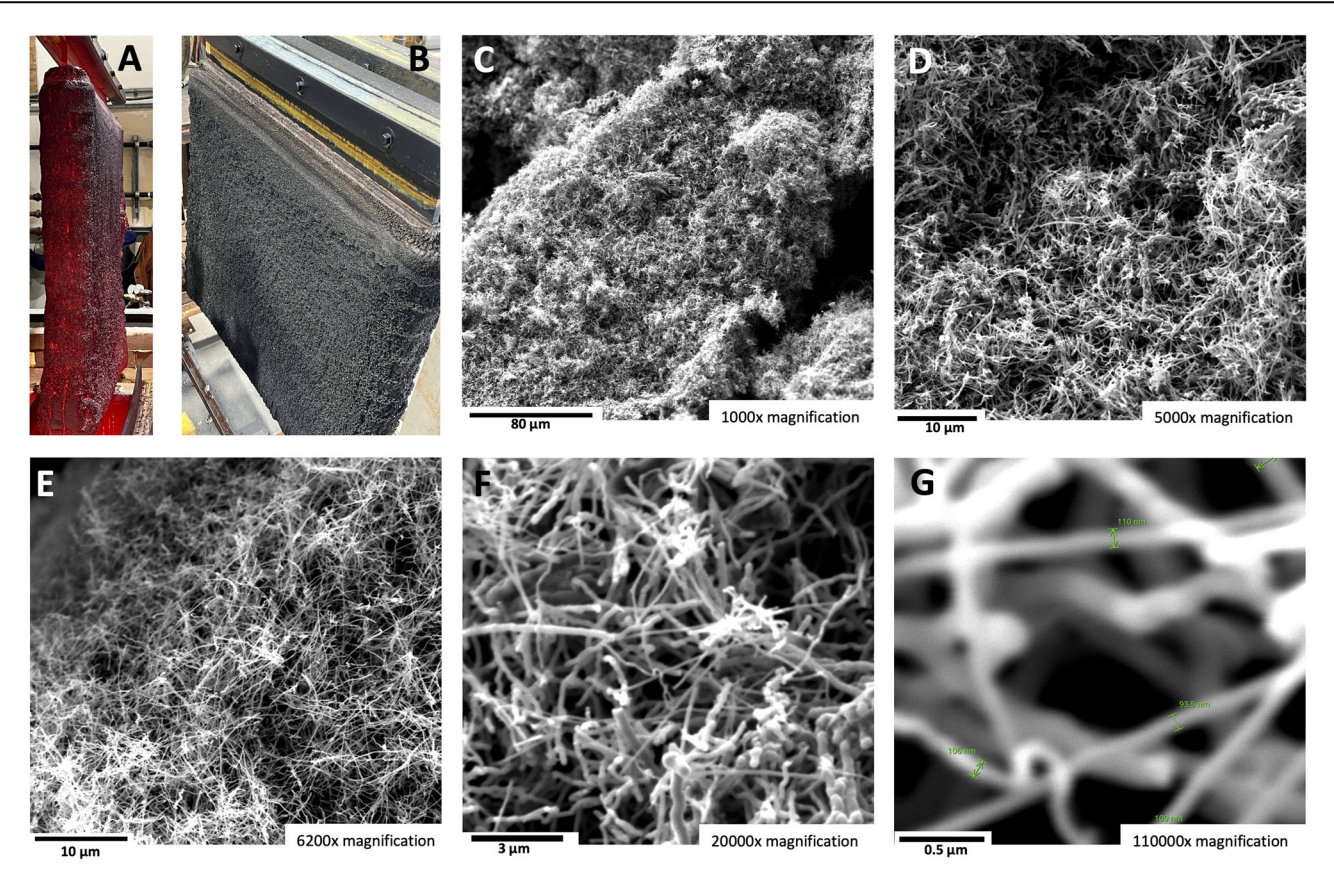


Fig. 8 | Carbon nanotube product with a high current density, large-area cathode, and 50 wt%  $SrCO_3/50$  wt%  $Li_2CO_3$  electrolyte. A, B show the cathode, with an active area of 11,000 cm<sup>2</sup>, upon lifting from the electrolyte and subsequent cooling.

**A** Electrolysis is conducted at 770 °C and J=0.6 A/cm² utilizing the stainless steel 304 carbon pot as the anode. The SEM product magnifications are as follows: C 1000×, D 5000×, E 6200×, F 20000×, G 11000× magnification.

solubility of strontium oxide adds another component to the electrolyte mix that can decrease the  $\rm Li_2CO_3$  component required in the electrolysis. As with  $\rm Li_2CO_3$ ,  $\rm Li_2O$  is an expensive lithium salt due to its scarcity and can be an expensive component to add to molten carbonate electrolytes. As with  $\rm SrCO_3$ ,  $\rm SrO$  is inexpensive and is an inexpensive additive to molten carbonate electrolytes for decarbonization.

We hypothesize that in the high strontium concentration domain, the addition of strontium oxide as a ternary compound to the binary SrCO $_3/$  Li $_2\mathrm{CO}_3$  system may improve mass transfer by increasing strontium solubility and decreasing viscosity. As shown in Fig. 10, a high-purity CNT product indeed formed at a low Li $_2\mathrm{CO}_3$  concentration and high SrCO $_3$  concentration upon the addition of SrO as a ternary component. The electrolysis was conducted in a 770 °C electrolyte at a current density of 0.6 A/cm². The 64 wt% SrCO $_3$  plus 1% SrO electrolyte contains only 35 wt% Li $_2\mathrm{CO}_3$ . The product continued to be high-purity CNTs, as had been observed with the lower concentration SrCO $_3$  electrolyses. As expected, with the addition of an oxide, the CNTs are more twisted but retain high purity. Interestingly, as shown in panels I and J, the diameter of the carbon nanotubes ranges from 70 to 90 nm, which is smaller than the 100 nm generally observed in electrolytes without added oxides.

## Ternary and quaternary SrCO<sub>3</sub> electrolytes with boron salts as little as 30% Li<sub>2</sub>CO<sub>3</sub>

We previously demonstrated that the addition of boron as a borate salt to lithium electrolyzed during molten carbonate electrolysis dopes CNTs, increasing the conductivity of the CNT product by an order of magnitude  $^{27,28,33}$ . Here, the effect of the addition of borax (Na<sub>2</sub>B<sub>4</sub>O<sub>7</sub>•10H<sub>2</sub>O) to a strontium-rich electrolyte on the purity of a carbon nanotube electrolysis product was investigated. Boraxes lose their water at temperatures greater than 602  $^{\circ}\text{C}^{57}$ . The electrolytes were probed in 75 wt% Li<sub>2</sub>CO<sub>3</sub>

electrolytes containing either 24/1, 22/3 or 20/5 wt%  $SrCO_3/wt\%$  borax. Electrolyses were conducted for 4 or 16 h at 0.6 A/cm² at 800 °C. Each yielded good quality CNTs according to SEM analysis, and their conductivity will be the topic of another study.

We hypothesize that in the high strontium concentration domain, the addition of strontium borate as a ternary compound to the binary SrCO<sub>3</sub>/ Li<sub>2</sub>CO<sub>3</sub> system may also improve mass transfer by increasing strontium solubility and decreasing the viscosity. In addition to adding another soluble component to the mixture, which tends to decrease the required Li<sub>2</sub>CO<sub>3</sub> required in electrolyte, in particular, we have observed that borate addition boron dopes and enhances the conductivity of the carbon nanotubes to facilitate the carbon nanotube growth 27,28,33. SrB<sub>4</sub>O<sub>7</sub> was synthesized by the reaction of SrCO<sub>3</sub> + 4H<sub>3</sub>BO<sub>3</sub> (boric acid), ground together, heat 4 h at 600 °C, reground, then heated overnight at 900 °C forming SrB<sub>4</sub>O<sub>7</sub> and confirmed by XRD. The electrolysis is conducted in 770 °C electrolyte at a current density of 0.6 A/cm<sup>2</sup>. As seen in Fig. 11, a high-purity CNT product is formed in this low 30 wt% Li<sub>2</sub>CO<sub>3</sub> concentration, and high 70 wt% Sr salt electrolyte. The product again continues to be the high-purity CNTs observed as those occurring as the product of lower concentration SrCO<sub>3</sub> electrolyses.

A straightforward quaternary SrCO $_3$  electrolyte also containing, only 30 wt% Li $_2$ CO $_3$  and boron, leads to the electrosynthesis of high-purity carbon CNTs. Rather than an initial step of the synthesis of SrB $_4$ O $_7$ , instead boron oxide (B $_2$ O $_3$  mp 450 °C) was added directly as a component in the electrolyte. Additionally, strontium oxide was added and the solid mix was heated to 800 °C for the electrolysis. Specifically, a 62 wt% SrCO $_3$ , 6 wt%  $_2^{\rm B}$ O $_3$  and 2 wt% SrO electrolyte contains only 30 wt% Li $_2$ CO $_3$ . Electrolysis was conducted in this electrolyte at 770 °C at current density of 0.6 A/cm² for 4 h. The product of this electrolysis are high-purity CNTs as shown by SEM in Fig. 12.

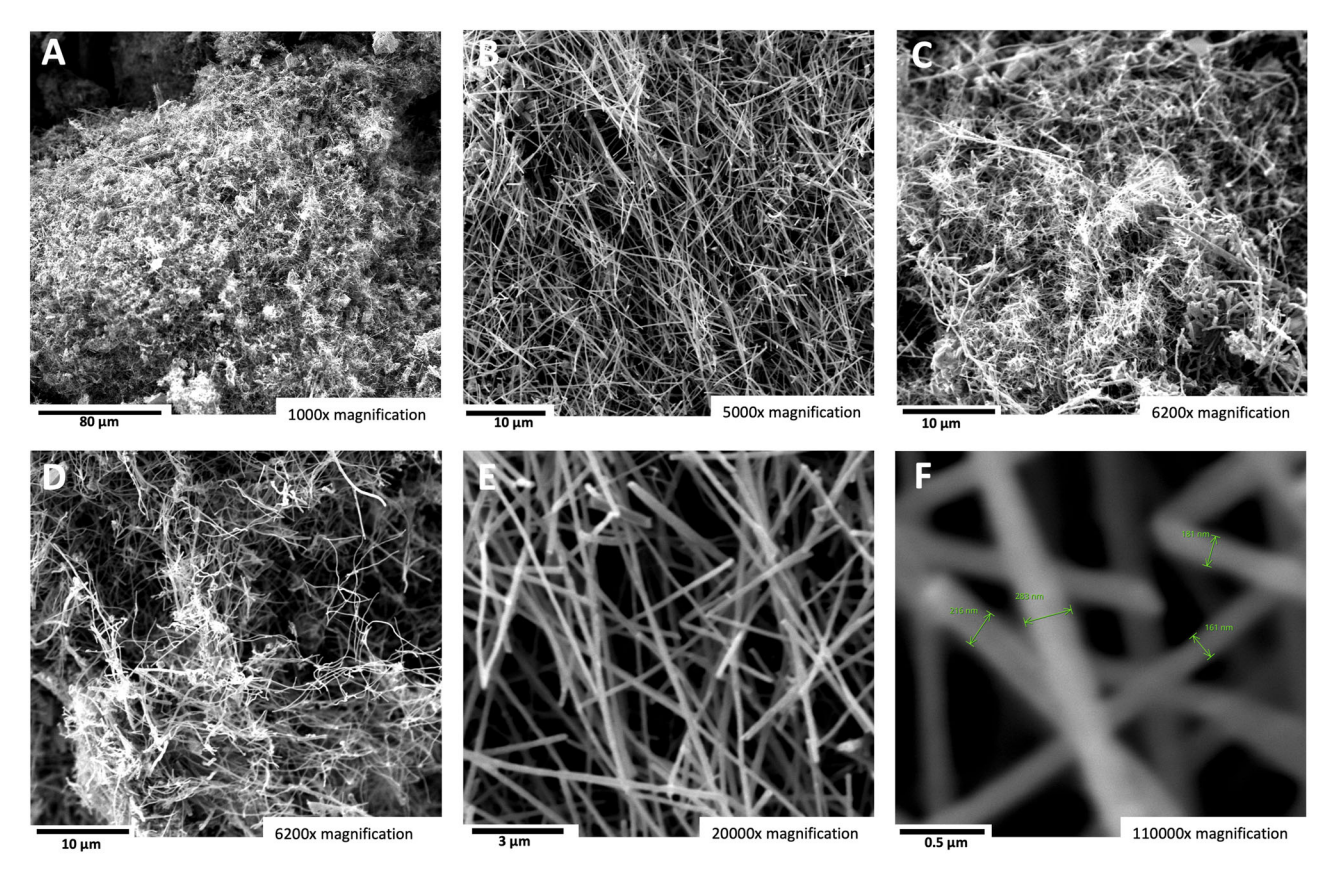


Fig. 9 | The carbon nanotube product of electrolysis in a 60 wt% SrCO<sub>3</sub>/40 wt% Li<sub>2</sub>CO<sub>3</sub> electrolyte. SEM images of the product from 16-h electrolysis conducted at 770 °C and J = 0.2 A/cm<sup>2</sup> with a stainless steel 304 anode at a 288 cm<sup>2</sup> area brass

cathode. The SEM magnifications are A 15500 $\times$ , B 5000 $\times$ , C 6200 $\times$ , D 6200 $\times$ , E 20,000 $\times$ , and F 110,000 $\times$ .

Ternary and quaternary  $30 \text{ wt} \% \text{ Li}_2\text{CO}_3$  electrolyte generates useful CNTs and are based on a readily available and underutilized SrCO<sub>3</sub> resource. The electrolytes represent a substantial cost reduction to a major component of the C2CNT decarbonization process.

## A nano-onion product and strontium electrolyte with sodium, barium, or boron salts

Interestingly, as shown in Fig. 13, an electrolyte with a low concentration of sodium carbonate can generate a high-purity carbon nano-onion (CNO) product rather than a CNT product. Using a lithium electrolyte without other alkali or alkali earth cations, we previously demonstrated the production of carbon nano-onions, such as in Li<sub>2</sub>CO<sub>3</sub> containing concentrated (5.9 m) Li<sub>2</sub>O<sup>34</sup>. As shown in the figure, we instead generated carbon nanoonions using a high strontium concentration electrolyte at 770 °C in a 41%/ 54%/5% lithium carbonate/strontium carbonate/sodium carbonate mixture at 0.6 A/cm<sup>2</sup>. Electrolysis (in the 3rd electrolysis run) generated >90% pure carbon nano-onion products. The percentage of carbon nano-onions in the product increased from 35% CNO after the first electrolysis to 65% CNO after the second electrolysis, to 65% CNO after the third electrolysis still occurred in the same electrolyte and yielded 95% pure CNO at the same electrodes (as shown in Fig. 13 panels B-F). Along with the CNOs, the third electrolysis product contained less than 1% CNTs as shown in panels B-F. A subsequent fourth electrolysis continued to yield similar high-purity CNOs. SEM image of a run of the electrolyte batch that had a lower CNO product is shown in Fig. 13 panel A. The results revealed a mixture of CNTs, CNO, and carbon nanobamboo products, indicating that the growth of the three GNC products was interrelated. The high-purity CNO product was also observed at 770 °C in the 65%/25%/10% lithium/strontium/sodium carbonate mixture at 0.2 A/cm<sup>2</sup>.

The carbon nano-onion product is also generated in the absence of sodium carbonate when electrolysis is perturbed, such as by lowering the cell temperature or by changing the electrolysis anode. For example, when a cell is lined with Nichrome A over the stainless steel of a carbon pot, the anode becomes Nichrome A (composition 80% Ni and 20% chrome), rather than 304 stainless steel, and iron is effectively excluded from the cell. We demonstrated that modifying and inhibiting transition metal nucleation can enhance carbon nano-onion formation <sup>34</sup>. Electrolysis in this Nichrome A anode cell at 770 °C electrolysis in 75%/25% lithium carbonate/strontium carbonate at 0.2 A/cm² produced 90% carbon nano-onions according to SEM inspection.

## Quinary and senary $SrCO_3$ electrolytes with as little as 20% $Li_2CO_3$

Sodium carbonate was added as an alternative ternary component to the strontium/lithium binary mixture, for the reason that Na<sub>2</sub>CO<sub>3</sub> adds an additional high solubility component to the electrolyte<sup>39</sup>, to probe alternative low lithium carbonate domains. A mixture comprising 1/3 of Li<sub>2</sub>CO<sub>3</sub>, 1/3 of SrCO<sub>3</sub>, and 1/3 of Na<sub>2</sub>CO<sub>3</sub> was fully molten at 750 °C, and at 750 °C, a 4-h electrolysis was conducted at 0.2 A/cm². The CNT product was of good quality and 80–90% purity according to inspection via SEM; although, it was not as high as the >> 90% purity evident in the unitary Li<sub>2</sub>CO<sub>3</sub> and binary or ternary Li<sub>2</sub>CO<sub>3</sub>/SrCO<sub>3</sub> electrolytes in Figs. 5–12. However, as expected from the sodium-containing electrolysis potentials in Fig. 2, the electrolysis potential was 0.6 V higher than that of the Na-free electrolytes. The 45 wt% Li<sub>2</sub>CO<sub>3</sub>, 45% SrCO<sub>3</sub>, 9 wt% Na<sub>2</sub>CO<sub>3</sub> and 1% Li<sub>2</sub>O<sub>2</sub> concentrations were again higher in voltage, and at 750 °C, 4 h of electrolysis at 0.4 A/cm² resulted in good quality CNT products at 85–90% purity.

A lower concentration of  $Na_2CO_3$ , along with a high concentration of  $SrCO_3$  electrolyte, facilitated CNT formation, albeit at a lower quality. This 770 °C electrolysis at  $0.6 \text{ A/cm}^2$  in 50%/45%/5% lithium carbonate/strontium carbonate produced 80% purity CNTs according to SEM inspection. The addition of 1% strontium oxide consistently yielded improved, good-

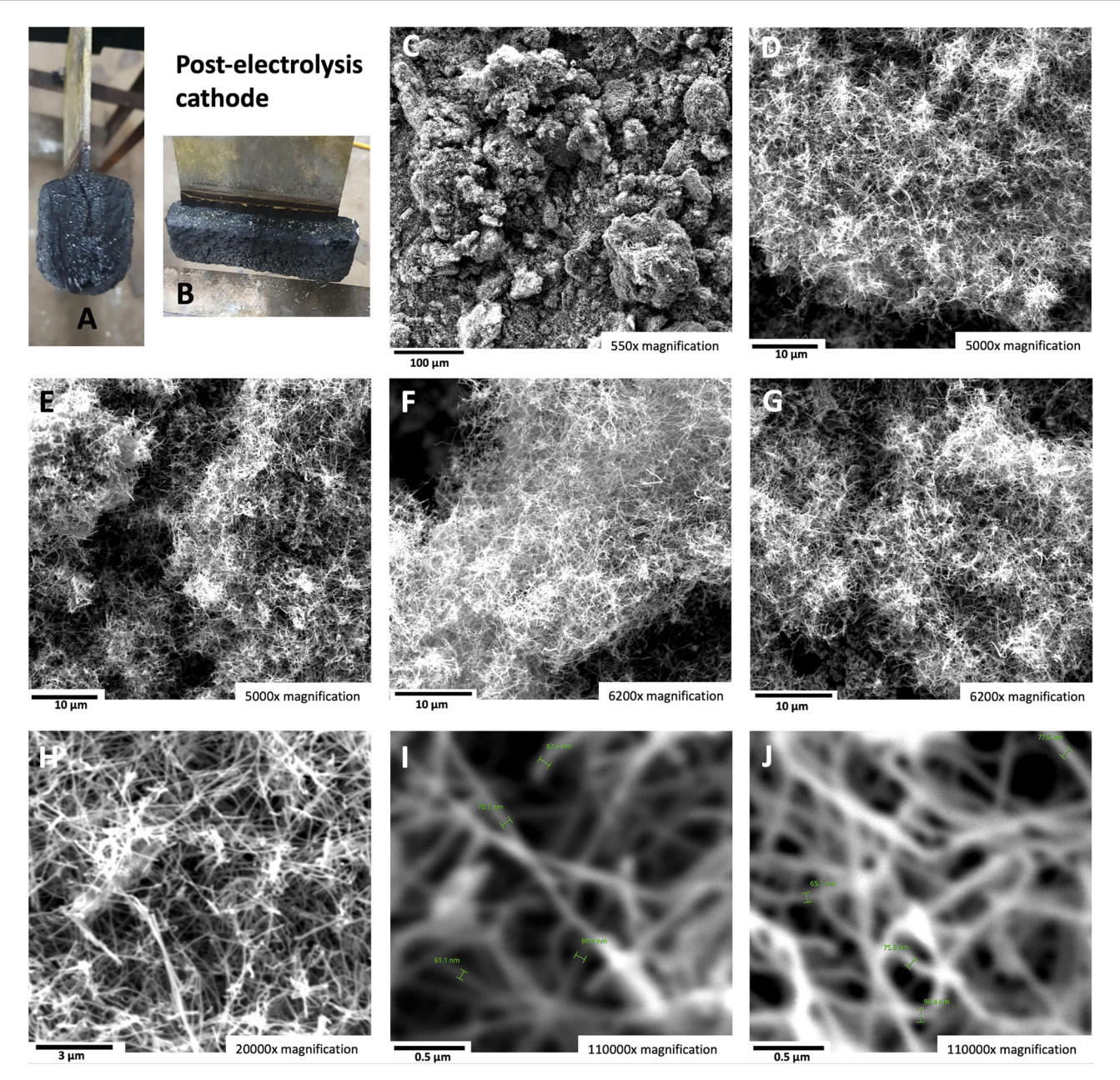


Fig. 10 | The carbon nanotube product of electrolysis in a ternary 35 wt%  $\rm Li_2CO_3$  electrolyte with 64 wt% SrCO $_3$  and 1 wt% SrO electrolyte. A, B Edge and top view of the 2-sided 6  $\times$  8 cm active area Muntz brass cathode with the post-electrolysis cooled product. C–J SEM images of the product from 4 h of electrolysis conducted at

770 °C and J = 0.6 A/cm<sup>2</sup> with a stainless steel 304 anode at a 96 cm<sup>2</sup> area brass cathode. The SEM magnification is **C**: 550×, **D**, **E**: 5000×, **F**, **G** 6200×, **H** 20,000×, or **I**, **J**: 110,000× magnification.

quality 85% purity CNT formation in 770 °C electrolytes at  $0.4 \, \text{or} \, 0.6 \, \text{A/cm}^2$  in 40%/50%/9% or in 40%/54%/5% lithium carbonate/strontium carbonate/sodium carbonate electrolytes containing 1 wt% strontium oxide.

Without added oxide, a 50% strontium carbonate electrolyte containing barium 25% carbonate did not produce CNOs nor CNTs (<10%); this electrolyte was electrolyzed at 770 °C and 25 wt% Li<sub>2</sub>CO<sub>3</sub>/50 wt% SrCO<sub>3</sub>/25 wt% BaCO<sub>3</sub> at 0.6 A cm². An electrolyte containing both sodium carbonate and barium oxide further increased the electrolysis potential by 0.1 V and generated <50% lower quality purity CNTs at 0.07, 10, 0.20, or 0.40 A/cm² in 40 wt% SrCO<sub>3</sub>, 40 wt% Li<sub>2</sub>CO<sub>3</sub>, 15 wt% Na<sub>2</sub>CO<sub>3</sub>, and 5 wt% BaO electrolyte at 775 °C.

The electrolytic splitting of CO<sub>2</sub> with electrolytes containing only 30% Li<sub>2</sub>CO<sub>3</sub>, such as the ternary and quaternary electrolyte mixture carbon nanotube products in Figs. 11, 12, achieve the goal in which low availability and expensive Li<sub>2</sub>CO<sub>3</sub> is no longer a major component of the molten

carbonate decarbonization system. A quinary electrolyte that contained only 30%  $\rm Li_2CO_3$  and split  $\rm CO_2$  to produce high-quality carbon nanotubes added strontium chloride to the electrolyte and contained wt% 20/57/5/2/6 of  $\rm Li_2CO_3/SrCO_3/2\%~SrO/B_2O_3$ . The synthesis at 800 °C used the same Muntz brass and 304 stainless electrodes and an electrolysis current density of  $\rm J=0.6~A/cm^2$  from 770 °C electrolysis in pure  $\rm Li_2CO_3$ 

It is expected, and observed that higher component electrolytes will have the capability to facilitate further dissolution of non-Li components in the molten carbonate decarbonization electrolyte, and thereby to lower lithium carbonate to less than 30. Such extended details should be pursued in further studies. Although this 30% objective has been reached, we will note here that we have further synthesized a high-quality carbon nanotube product with a quinary (5 component) 25% Li<sub>2</sub>CO<sub>3</sub> 800 °C electrolyte consisting of wt% 25/62/5/2/6 of Li<sub>2</sub>CO<sub>3</sub>/SrCO<sub>3</sub>/Na<sub>2</sub>CO<sub>3</sub>/SrO/B<sub>2</sub>O<sub>3</sub> under the same 800 °C electrolysis conditions. In another quinary electrolyte

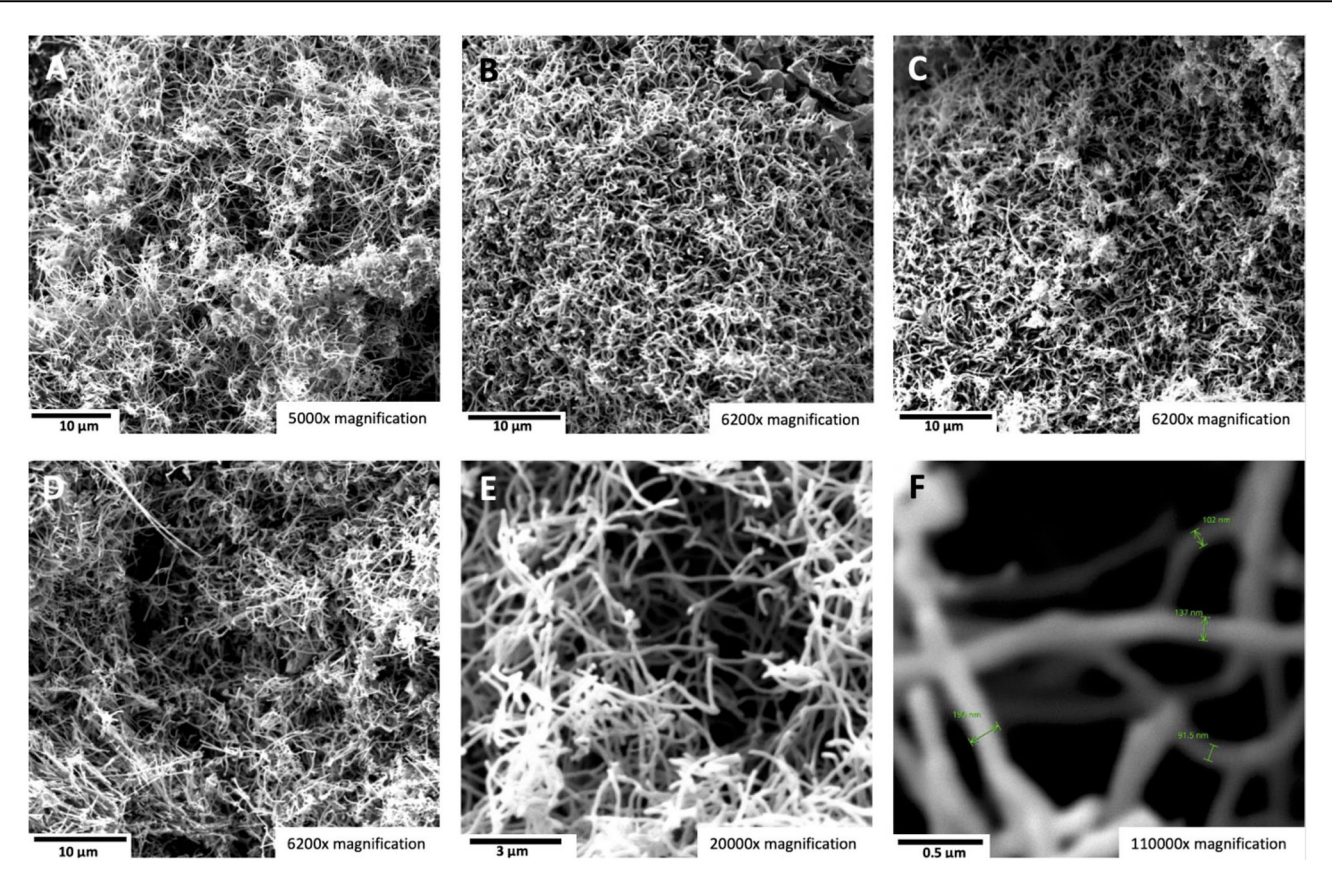


Fig. 11 | The carbon nanotube product of an electrolysis in a ternary 30 wt%  $\text{Li}_2\text{CO}_3$  electrolyte with 60 wt%  $\text{SrCO}_3$  and 10 wt%  $\text{SrB}_4\text{O}_7$  electrolyte. A–E SEM of the product from the 4-h electrolysis conducted at 770 °C and J = 0.6 A/cm<sup>2</sup> with a

stainless steel 304 anode at a 96 cm $^2$  area brass cathode. The SEM magnification is: A 5000×, B–D 6200×, E 20,000×, or F 110,000× magnification.

producing a good CNT product, we have further decreased the  $\rm Li_2CO_3$  content to 20% with an electrolyte of  $\rm 20/62/10/2/6$  of  $\rm Li_2CO_3/SrCO_3/Na_2CO_3/SrO/B_2O_3$ . Finally, in a senary (six component) electrolyte producing a good CNT product under the same electrolysis conditions consists of wt%  $\rm 20/57/10/2/6/5~Li_2CO_3/SrCO_3/Na_2CO_3/SrCl_2/SrO/B_2O_3$ .

#### Cost analysis of C2CNT decarbonization

This brief analysis draws comparisons with the cost structure of a well-established industry: aluminum production. The C2CNT process shares several characteristics with aluminum smelting. Both involve molten electrolysis and do not require noble or exotic materials. Aluminum smelting converts aluminum oxide into aluminum metal, while C2CNT produces carbon nanotubes from carbon dioxide. Aluminum smelting operates at around 960 °C in a molten cryolite (sodium fluoroaluminate) electrolyte, while C2CNT operates in molten carbonate. Both processes function at high current densities (hundreds of mA per cm²) and exhibit low polarization. The electrolysis chambers in both processes are constructed from common metals, standard insulators (such as kiln or "firebricks"), and control equipment. In aluminum smelting, electrolysis is driven at approximately 4 volts, utilizing 3 electrons per aluminum atom.

A summary of Al production costs per tonne of Al, based on market costs, is presented in Table 1. These costs are averaged from similar values in several studies <sup>58-62</sup>. The \$2005 in costs are consistent with today's market value of \$2400 per tonne of aluminum<sup>63</sup>. The costs consist of: Consumable Expenses including materials (52% including alumina, carbon, and cryolite), Electricity: 32%, Labor: 8%, and Capital Expenses (amortized cost of electrolyzers, processing equipment, and miscellaneous overhead). For each tonne of aluminum, the production consumes 5.69 tonnes of alumina (refined bauxite), 0.40 tonne of carbon, and 0.126 tonnes of cryolite<sup>62</sup>. Note

that the energy required for aluminum production comes from two sources: electricity and the energy released from the consumed carbon anode.

As shown in Table 1, the C2CNT process differs from aluminum smelting in that it uses a low-cost oxide—carbon dioxide—rather than aluminum oxide (alumina processed from NaOH-treated bauxite). Both processes are straightforward, high-current-density electrochemical methods involving molten electrolytic reduction of oxides. The C2CNT process operates under somewhat milder conditions at approximately 770 °C in a less toxic, molten carbonate electrolyte, and to a first order of approximation, both processes will be assumed to have the same labor costs, tonnage of electrolyte consumption, and capital costs. Whereas, Al production requires ~13 MWh per ton of aluminum at \$0.05/kWh, C2CNT production requires less energy (7 MWh) per ton of carbon nanotubes based on the 4-electrons per carbon dioxide splitting. The electrolysis voltage varies from 0.8 V to up to 2 V1,2, and an electrical cost of \$360 per ton CNT. A major difference in the cost structure is based on electrolyte cost. Whereas costs are ~\$1000 per tonne cryolite<sup>64</sup>, and ~\$1040 per tonne strontium carbonate<sup>45</sup>, lithium carbonate costs are ~\$15,000 per tonne 46. For the 0.126 tonne of electrolyte, this yields comparative total tonnage costs of \$2005 for aluminum, only \$791 per tonne for CNTs based on the SrCO<sub>3</sub> (note high, but not 100%, SrCO<sub>3</sub> electrolyte was demonstrated in this study), and \$2610 per tonne based on the Li<sub>2</sub>CO<sub>3</sub> electrolyte. These CNT will fluctuate with the large variation in Li<sub>2</sub>CO<sub>3</sub> cost and the electrolyte waste per tonne of CNT produced (which is assumed here as similar to that of Al production). Note, that the dominant cost in CNT production is the electrolyte and total costs for CO<sub>2</sub> splitting to carbon nanotubes are over 3-fold higher for the lithium carbonate compared to the new strontium carbonate chemistries. Substantial fluctuations in lithium carbonate due to growing EV demand can further exacerbate this price differential.

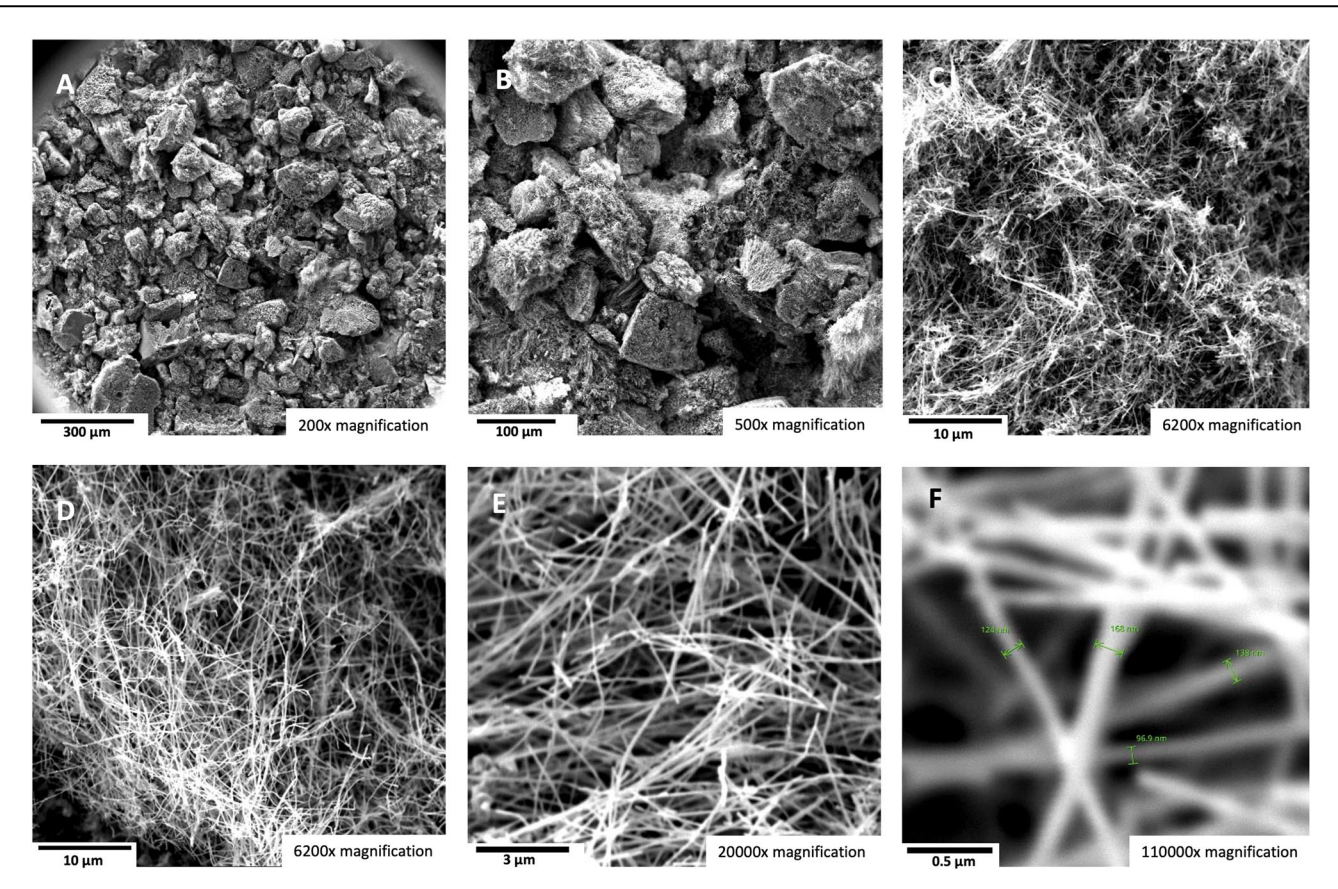


Fig. 12 | The carbon nanotube product of an electrolysis in a quaternary 30 wt%  $\text{Li}_2\text{CO}_3$  electrolyte with 62 wt%  $\text{SrCO}_3$ , 6 wt%  $\text{B}_2\text{O}_3$  and 2 wt% SrO electrolyte. A–E SEM of the product from the 4-h electrolysis conducted at 770 °C and J=0.6 A/

cm² with a stainless steel 304 anode at a 96 cm² area brass cathode. The SEM magnification is: A 200 $\times$ , B 500 $\times$ , C, D 6200 $\times$ , E 20,000 $\times$ , or F 110,000 $\times$  magnification.

The value of carbon nanotubes is considerably higher than that of aluminum or the estimated C2CNT production costs in Table 1. The large price range reflects the different costs of industrial compared to high purity grade carbon nanotubes<sup>65</sup>. Carbon nanotubes have found applications in materials such as medicine, polymers, batteries, cement, and textiles<sup>13–23</sup>. A principal advantage of the C2CNT process is that the graphene nanocarbon products are made from CO<sub>2</sub>. With the larger diameter C2CNT CNTs, there is a greater number of concentric cylindrical walls of graphene. These increased-diameter CNTs exhibit a propensity for higher electrical and thermal conductivity, greater rigidity, enhanced electromagnetic radiation absorption, and better (Li-ion) charge storage. The high electrical storage capacity of C2CNT synthesized CNTs has been demonstrated<sup>29</sup>, their use in strengthened polymers presented<sup>66</sup>, and synthesis procedures for doped, helical, magnetic, thin, thick, tangled, straight, long, and bamboo and pearl morphology hollow core CNTs presented<sup>45,5,27,28,30–33</sup>.

#### **Conclusions**

We have presented in this study a sustainability advance in decarbonization technology to directly address global warming, and removal of the greenhouse gas carbon dioxide. The molten  ${\rm Li_2CO_3}$  transformation of  ${\rm CO_2}$  to oxygen and graphene nanocarbons, is a large scale process of  ${\rm CO_2}$  removal to mitigate climate change. Sustainability benefits include the stability and storage of the products, and the GNC product value is an incentive for carbon removal. However, the high cost of the  ${\rm Li_2CO_3}$  electrolyte and its competitive use as the primary raw material for EV batteries are obstacles.

Lithium carbonate is less available than strontium carbonate, both due to its lower natural abundance and because of the increasing demand for lithium carbonate for EVs and Li-ion batteries. The high cost of lithium carbonate has been suggested as an impediment to molten carbonate decarbonization by C2CNTs. The carbonate carbonization electrolytes

prepared from concentrated strontium carbonate demonstrated in this study are substantially more cost-effective than lithium-based electrolytes. The incompatibility of the high solidus point of  $\rm SrCO_3$  with the preferred molten carbonate decarbonization range of  $<\!800\,^{\circ}\rm C$  has been overcome by determining that strontium carbonate is unusually soluble (to 65% at 790 °C in lithium carbonate). Ternary or higher carbonate mixed electrolytes can further decrease the lithium concentration in the carbonate electrolyte. The thermodynamic equilibrium for the affinity of strontium carbonate to absorb and release carbon dioxide was calculated and shown to be comparable to that of lithium carbonate and shown to be substantially different from that of the other corresponding alkali and alkali earth carbonate equilibria.

The use of a low-Li electrolyte that can provide an electrolyte melting point within the optimal C2CNT process range for  $\rm CO_2$  to GNC growth between approximately 700 °C and approximately 800 °C has been investigated for concentrated strontium carbonate electrolytes. The electrochemical potential of molten carbonate electrolysis was investigated, and the results showed that the electrolysis potential is low for both pure lithium and binary strontium/lithium electrolytes but higher for sodium or barium carbonate electrolytes.

Low-lithium electrolysis was performed using a vertical planar Muntz brass, cathode and vertical anodes composed of stainless steel. Effective high-concentration strontium-based electrolytes that produce high-quality GNC products include both binary mixtures (for example, strontium carbonate/lithium carbonate or strontium oxide/lithium carbonate) and ternary mixture electrolytes (for example, strontium carbonate/lithium carbonate/strontium oxide or borate or sodium salts).

A high current density of 0.6 A/cm<sup>2</sup> is consistent with industrial-rate electrochemical processes. Binary and ternary strontium carbonate electrolytes were systematically probed for CO<sub>2</sub> electrolytic decarbonization. At

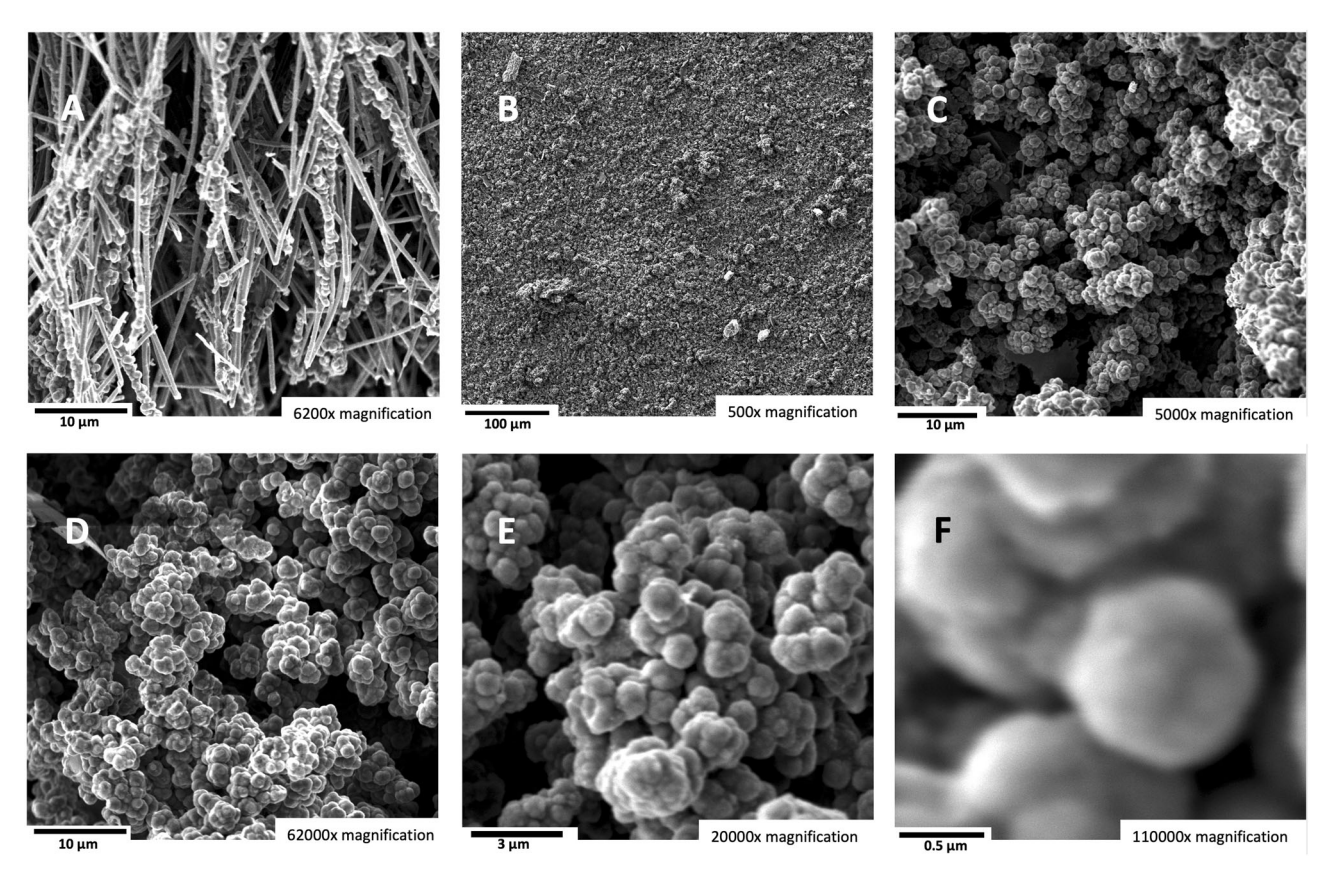


**Fig. 13** | Strontium with sodium carbonate electrolyte produces carbon nanonions. A shows an SEM image of a lower CNO product purity previously grown in the same electrolyte, which shows a mixture of CNTs, CNO, and carbon nanobamboos. Panels (**B**) through (**G**) show the SEM images of a product with a pure CNO product. Electrolyses were conducted in 54 wt% SrCO<sub>3</sub>, 41 wt% Li<sub>2</sub>CO<sub>3</sub>, and

5 wt%  $Na_2CO_3$  in an electrolyte at 770 °C and  $J=0.6~A/cm^2$  utilizing a stainless steel 304 carbon pot as the anode and a 168 cm² area brass cathode. The SEM magnifications are **A** 6200×, **B** 500×, **C** 5000×, **D** 6200×, **E** 20,000×, and **F** 110,000× magnification.

Table 1 | Comparison of aluminum and C2CNT production costs and value per tonne product

Process	\$US Cost (% of total)							product	Price/tonne
Al smelt	Reactant	carbon	electrolyte	electricity	labor	capital	total	_	
	alumina 733 (37%)	\$211 (12%)	Cryolite \$126 (6%)	\$602 (30%)	\$150 (7%)	\$150 (7%)	\$2005 (100%)	aluminum metal	\$2,400
C2CNT (SrCO <sub>3</sub> )	CO <sub>2</sub> (0%)	0 (0%)	SrCO <sub>3</sub> \$131 (17%)	\$360 (46%)	\$150 (19%)	\$150 (19%)	\$791 (100%)	carbon nanotubes	\$40.000-\$1,000,000
C2CNT (Li <sub>2</sub> CO <sub>3</sub> )	\$0 (0%)	0 (0%)	Li <sub>2</sub> CO <sub>3</sub> \$1950 (75%)	\$360 (14%)	\$15 (6%)	\$150 (6%)	\$2610	carbon nanotubes	\$40.000-\$1,000,000

770 °C and a high current density of  $0.6\,\mathrm{A/cm^2}$ ,  $64\,\mathrm{wt\%}~\mathrm{SrCO_3}$ ,  $35\,\mathrm{wt\%}~\mathrm{Li_2CO_3}$ , and 1 wt% SrO are among those demonstrated to be effective for high-purity carbon nanotube electrosynthesis and substantially decrease the concentration of lithium carbonate required in the electrolyte. Another concentrated strontium carbonate electrolyte, consisting of  $54\,\mathrm{wt\%}~\mathrm{SrCO_3}$ ,  $41\,\mathrm{wt\%}~\mathrm{Li_2CO_3}$ , and  $1\,\mathrm{wt\%}~\mathrm{SrO}$ , is effective for high-purity carbon nanonion production.

### Methods

#### Materials

Lithium carbonate was purchased at a battery grade >99.5% and was used as received. The lithium carbonate had a compositional composition of 99.8% (Li<sub>2</sub>CO<sub>3</sub>, Green Chemical Co.). The strontium carbonate used was 99.4% pure SrCO<sub>3</sub> (Shendong Zhi Chemical Co. Strontium oxide, SrO (99% purity, Chemsavers) was used as an electrolyte component in this study. A lower purity SrCO<sub>3</sub> (98.6%; Hengshui Haoye Co.) tested, containing minor ternary mixture components (0.8% BaCO<sub>3</sub> and 0.2 wt% CaCO<sub>3</sub>) and had

comparable solubility to the higher grade  $SrCO_3$  shown in the solubility section.  $BaCO_3$  (Alfa Aesar, 99.5%),  $Na_2CO_3$  (Alfa Aesar, 99%),  $Li_2O$  (Alfa Aesar, 99.5%), and BaO (Alfa Aesar, 97%) are also combined to form various molten electrolytes.

Muntz brass (0.25 inches thick in <2000 cm² electrolyses and 0.5 inches thick in the larger cathode study) is a high-zinc brass alloy composed of 60% copper and 40% zinc; this material is also referred to as 280 brass. This material serves as the cathode and was purchased from onlinemetals.com and in larger quantities from Marmetal Industries. Electrolysis was conducted in 304 stainless steel "carbon pots". The pot acts as both the cell case and its inner walls serve as the anode. In one case, as delineated in the text, the inner wall of the pot was lined with Nichrome A to serve as an alternative electrolysis anode.

#### **Electrolysis and purification**

The specific electrolyte compositions are premixed by weight at the noted ratios for each of the electrolytes described. For the electrolysis potential measurements, the electrolyte to be studied was melted at  $770\,^{\circ}$ C in a small



Fig. 14 | The Genesis Device\* kiln used for large-scale CO2 molten carbonate electrolysis. The decarbonization kilns are onsite at Carbon Corp in Calgary, Canada.

 $(12 \text{ cm} \times 1 \times 2 \text{ cm} \times 15 \text{ cm} \text{ tall})$  304 stainless steel. A 0.2 cm wide, 1.5 cm long Muntz brass cathode wire was placed 3 mm from a flat, oversized  $(3 \text{ cm} \times 6 \text{ cm})$  304 stainless steel anode and immersed in the electrolyte. Electrolysis potentials were measured. Fixed galvanostatic currents were applied, and electrolysis was measured via a DataQ DAQ interface.

For the electrolysis experiments, a variety of 304 stainless steels were used. In each case, the cathode is mounted vertically in the electrolyte and across the carbon pot wall, serving as an anode and immersed. Large cathodes, such as those pictured in Figs. 1, 8, are maintained in large thermostatically controlled kilns, as shown in Fig. 14. These kilns simultaneously sustain electrolysis in several carbon pots. The electrolyte has a strong affinity for CO<sub>2</sub> from the open air, and air was used as the CO<sub>2</sub> source. The kilns shown in Fig. 14 can also be configured for effective use as an alternative CO<sub>2</sub> source and direct feed of 5% CO<sub>2</sub> emissions from the adjacent 860 MW (Shepard, Calgary Canada) natural gas electric power plant. The electrodes are immersed subsequent to electrolyte melt. Once melted, the electrolyte under investigation was maintained at 750 °C to 800 °C, as noted in the text and the figure legends. Electrolysis was conducted galvanostatically with a constant current density. CO<sub>2</sub> is transformed to carbon, and grows at the cathode as a carbanogel containing a matrix of graphene nanocarbons (GNCs) and a molten electrolyte.

After electrolysis, the raw product from the cathode is cooled, collected from the cathode, ground, remelted, pressed and/or washed with aqueous acid. The washed carbon product was separated by vacuum filtration. The washed carbon product was dried overnight at 60 °C in an oven, yielding a black powder product.

Details of the pressing procedure used to remove excess electrolyte from the product are available <sup>67,68</sup>. This study focused on the optimization of the electrolyte conditions, and for that purpose, a cooled carbanogel containing electrolyte removed from the cathode was retained for use. The hot carbanogel containing molten electrolyte may be pressed directly from the still-hot cathode. This will be shown in subsequent studies.

#### Characterization

The carbon products were washed and analyzed by PHENOM Scanning Electron Microscopy and TGA, and is in conjunction with TEM, TEM HAADF, Raman, and XRD, we previously characterized the carbon nanotube products as detailed in the Supplementary Material. In this case, the product purity from 770 °C electrolysis in pure Li<sub>2</sub>CO<sub>3</sub> is high-purity multiwalled carbon nanotubes. The CNT walls and the CNT hollow cores are evident in panels A and D of supplementary SI Fig. S2. The CNT tip is comprised of carbon, surrounding the nucleation metals of iron with a smaller concentration of nickel in panels C. At higher TEM magnification,

the individual, concentric graphene walls are, shown separated by the representative 0.34 nm inter-graphene layer spacing in A-1 panels B1-1, and the pure carbon composition of the CNT cross-section is presented in the bottom righthand panel of Fig. S2. As previously delineated, the CNT diameter and number of graphene walls initially increases with growth time and approaches a limiting diameter<sup>36</sup>. Presumably, the limiting diameter occurs as the nucleating transition metal becomes increasingly buried within the CNT tip. This limit will depend on electrochemical conditions<sup>30</sup>. As one example, after 5, 15, or 90 min of electrolytic growth, the hollow core CNTs grew respectively from 18 to 39 to 142 graphene walls and respectively of 22, 47 to 116 nm diameters in molten 770 °C Li<sub>2</sub>CO<sub>3</sub><sup>36</sup>. SEM, shown in Fig. 5, were performed with a PHENOM Pro-X SEM (with Energy Dispersive Spectroscopy, EDS), and Figs. 6-11 were measured with a PHE-NOM Pro-XL High THROUGHPUT SEM. TGA were performed with a Perkin Elmer STA 6000 TGA/DSC instrument with autosampler instrumentation.

#### **Data availability**

The source data that support the findings of this study are available from the corresponding authors upon reasonable request. Source data are provided within this paper and in the Supplementary Material.

Received: 17 July 2024; Accepted: 11 September 2024; Published online: 18 September 2024

#### References

- Ren, J., Li, F.-F., Lau, J., Gonzalez-Urbina, L. & Licht, S. One-pot synthesis of carbon nanofibers from CO<sub>2</sub>. Nano Lett. 15, 6142–6148 (2015).
- Ren, J., Lau, J., Lefler, M. & Licht, S. The minimum electrolytic energy needed to convert carbon dioxide to carbon by electrolysis in carbonate melts. J. Phys. Chem. C. 119, 23342–23349 (2015).
- Ren, J. & Licht, S. Tracking airborne CO<sub>2</sub> mitigation and low cost transformation into valuable carbon nanotubes. Sci. Rep. 6, 27760–27761–11 (2016).
- Liu, X., Licht, G. & Licht, S. Controlled transition metal nucleated growth of unusual carbon allotropes by Molten Electrolysis of CO<sub>2</sub>. Catalysts 12, 125 (2023).
- Liu, X., Licht, G. & Licht, S. Controlled transition metal nucleated growth of carbon nanotubes by Molten Electrolysis of CO<sub>2</sub>. Catalysts 12, 137 (2023).
- Liu, B. & Ma, S. Precise synthesis of graphene by chemical vapor deposition. *Nanoscale* 16 4407–4433 (2024).

- Singh, M. V., Tiwari, A. K. & Gupta, R. Catalytic chemical vapor deposition methodology for carbon nanotubes synthesis. *Chem. Sel.* 8, e202204725 (2023).
- Pant, M., Singh, R., Negi, P., Singh, R. & Tiwari, K. A comprehensive review on carbon nanotube synthesis using chemical vapor deposition. *Materials Today, Proc.* 46, 11250–11253 (2021).
- Sivamaran, V. et al. Carbon nanotubes, nanorings, and nanospheres: synthesis and fabrication via chemical vapor deposition—a review. Nanomater. Nanotechnol. 12 https://doi.org/10.1177/1847980422 1079495 (2022).
- Manawi, Y. M., Ihsanullah, Samara, A., Al-Ansari, T. A. & Atieh, M. A review of carbon nanomaterials' synthesis via the chemical vapor deposition (CVD) method. *Materials* 11, 1050833 (2018).
- Khanna, V., Bakshi, B. R. & Lee, L. J. Carbon Nanofiber Production: Life cycle energy consumption and environmental impact. *J. Ind. Ecol.* 12, 394–410 (2008).
- Xie, Z. et al. CO<sub>2</sub> fixation into carbon nanofibers using electrochemical-thermochemical tandem catalysis. *Nat. Catal.* 7, 98–109 (2024).
- 13. NanoCarbon: A Wonder Material for Energy Applications. Gupta, R. K., Ed. Springer, Singapore (2024).
- Speranza, G. Carbon nanomaterials: synthesis, functionalization and sensing applications. *Nanomat* 11, 967 (2021).
- Brito, C. L. et al. A review on carbon nanotubes family of nanomaterials and their health field. ACS Omega 9, 8687–8708 (2024).
- Ali, Z. et al. Critical review on the characterization, preparation, and enhanced mechanical, thermal, and electrical properties of carbon nanotubes and their hybrid filler polymer composites for various applications. Compos. Part C. 13, 100434 (2024).
- Rahman, M. M., Asiri, A. M. & Chowdhury, M. A., Carbon Nanotubes -Recent advances, new perspectives and potential applications (IntechOpen, London, 2023).
- 18. Guo, H.-L. et al. Properties and defense applications of carbon nanotubes. *J. Phys. Conf. Ser.* **2478**, 042010 (2023).
- Maheswaran, R. & Shanmugavel, B. P. A critical review of the role of carbon nanotubes in the progress of next-generation electronic applications. J. Electron. Mat. 51, 2787–2800 (2022).
- Rao, R. K., Gauttham, S. & Sasmal, S. A comprehensive review on carbon nanotubes based smart nanocomposites sensors for various novel sensing applications. *Polymer Rev.* 64, 575–638 (2024).
- Cai, Y. et al. Application and structure of carbon nanotube and graphene-based flexible electrode materials and assembly modes of flexible lithium-ion batteries toward different functions. Front. Carbon https://doi.org/10.1007/s11708-024-0911-2 (2024).
- Nimthra, K. C., Fiji, A., George, T. M., Henri, V., Maria, H. J. & Thomas, S. Carbon nanotube filled rubber nanocomposites. *Front. Carbon* 3, 1–19 (2024).
- Bajad, M. N. Cement-based composites containing carbon nanofibers and carbon nanotubes. Curr. Mat. Sci. 17, 240–250 (2024).
- Ahlawat, J. et al. Application of carbon nano onions in the biomedical field- recent advances and challenges. *Biomater. Sci.* 9, 626–666 (2020).
- Vindhyasarumi, A. et al. A comprehensive review on recent progress in carbon nano-onion based polymer nanocomposites. *Eur. Polym. J.* 194, 112143 (2023).
- Kausar, A. & Ghavanloo, E. Carbon nano-onions reinforced nanocomposites: fabrication, computational modeling techniques and mechanical properties Solid State. Mat. Sci. 50, 2322954 (2024).
- Johnson, M. et al. Carbon nanotube wool made directly from CO<sub>2</sub> by molten electrolysis: value driven pathways to carbon dioxide greenhouse gas mitigation. *Mater. Today, Energy* 5, 230–236 (2017).
- Johnson, M. et al. Data on SEM, TEM and Raman spectra of doped, and helic carbon nanotubes made directly from CO<sub>2</sub> by molten electrolysis. Data Br. 14, 592–606 (2017).

- Licht, S. et al. Carbon nanotubes produced from ambient carbon dioxide for environmentally sustainable lithium-ion and sodium-ion battery anodes. ACS Cent. Sci. 2, 162–168 (2016).
- Wang, X., Liu, X., Licht, G. & Licht, S. Calcium metaborate induced thin walled carbon nanotube syntheses from CO<sub>2</sub> by molten carbonate electrolysis. Sci. Rep. 10, 15146 (2020).
- Liu, X., Licht, G. & Licht, S. The green synthesis of exceptional braided, helical carbon nanotubes and nanospiral platelets made directly from CO<sub>2</sub>. Mat. Today, Chem. 22, 100529 (2021).
- 32. Wang, X. et al. Magnetic carbon nanotubes: carbide nucleated electrochemical growth of ferromagnetic CNTs from CO<sub>2</sub>. *J. CO2 Util.* **40**, 101218 (2020).
- Ren, J., Johnson, M., Singhal, R. & Licht, S. Transformation of the greenhouse gas CO<sub>2</sub> by molten electrolysis into a wide controlled selection of carbon nanotubes. *J. CO2 Util.* 18, 335–344 (2017).
- Liu, X., Ren, J., Licht, G., Wang, X. & Licht, S. Carbon nano-onions made directly from CO<sub>2</sub> by molten electrolysis for greenhouse gas mitigation. Adv. Sustain. Syst. 3, 1900056 (2019).
- Wang, X., Licht, G., Liu, X. & Licht, S. One pot facile transformation of CO<sub>2</sub> to an unusual 3-D nan-scaffold morphology of carbon. *Sci. Rep.* 10, 21518 (2020).
- Liu, X., Wang, X., Licht, G. & Licht, S. Transformation of the greenhouse gas carbon dioxide to graphene. J. CO2 Util. 36, 288–294 (2020).
- 37. Wu, H. et al. One-pot synthesis of nanostructured carbon materials from carbon dioxide via electrolysis in molten carbonate salts. *Carbon* **106**, 208–217 (2016).
- 38. Licht, S. Stabilization of STEP electrolyses in lithium-free molten carbonates. arXiv: 1209.3512 [physics.chem-ph] (2012).
- 39. Wang, X., Liu, X., Licht, G., Wang, B. & Licht, S. Exploration of alkali cation variation on the synthesis of carbon nanotubes by electrolysis of CO₂ in molten carbonates. *J. CO2 Util.* **18**, 303–312 (2019).
- 40. Licht, S., Cui, B. & Wang, B. STEP carbon capture the barium advantage. *J. CO2 Util.* **2**, 58–63 (2013).
- Licht, S. et al. STEP cement: solar thermal electrochemical production of CaO without CO<sub>2</sub> emission. *Chem. Commun.* 48, 6019–6021 (2012).
- 42. Licht, S. Coproduction of cement and carbon nanotubes with a carbon negative footprint. *J. CO2 Util.* **18**, 378–389 (2017).
- Licht, G., Wang, X., Liu, X., Licht, S. CO<sub>2</sub> Utilization by electrolytic splitting to carbon nanotubes in non-lithiated, cost-effective, molten carbonate electrolytes. *Adv. Sustain. Syst.* 6, 2100481 (2022).
- 44. Ptacek, P. et al. The kinetics and mechanism of thermal decomposition of SrCO3 polymorphs. *Ceram. Int.* **41**, 115–126 (2015).
- Carbonates; Strontium Carbonate Price, Source: https://www. indexbox.io/search/carbonates-strontium-carbonate-price-china/# (last accessed August 19, 2024).
- Lithium carbonate prices, source: https://tradingeconomics.com/ commodity/lithium (last accessed April 22, 2024).
- McDonough, W. F. Earth's Core. In: White, W. (eds) Encyclopedia of Geochemistry. Encyclopedia of Earth Sciences Series. Springer, Cham (2017).
- 48. Yang, J. et al. Hydrothermal synthesis of SrCO3: Eu3þ/Tb3þ microneedles and their luminescence properties. *J. Cryst. Growth* **303**, 480–486 (2007).
- Tipcompor, N., Thongtem, T., Phuruangrat, A. & Thongtem, S. Characterization of SrCO<sub>3</sub> and BaCO<sub>3</sub> nanoparticles synthesized by cyclic microwave radiation. *Mater. Lett.* 87, 153–156 (2012).
- Garcés, R. S., Torres, J. T. & Valdés, A. F. Synthesis of SrAl2O4 and Sr3Al2O6 at high temperature, starting from mechanically activated SrCO3 and Al2O3 in blends of 3:1 molar ratio. *Ceram. Int.* 38, 889–894 (2012).
- Hazeli, K., Sadeghi, A., Pekguleryuz, M. O. & Kontsos, A. The effect of strontium in plasticity of magnesium alloys. *Mater. Sci. Eng. A* 578, 383–393 (2013).

- Niu, J.-X., Chen, Q.-R., Xu, N.-X. & Wei, Z.-L. Effect of combinative addition of strontium and rare earth elements on corrosion resistance of AZ91D magnesium alloy. *Trans. Nonferr. Met. Soc. China* 18, 1058–1064 (2008).
- 53. Odler, I. Special Inorganic Cements, Taylor & Francis, New York (2004).
- Chatterjee, A. K. Re-examining the prospects of aluminous cements based on alkali-earth and rare-earth oxides. *Cem. Concr. Res.* 39, 981–988 (2009).
- Ptáček, P., Soukal, F., Opravil, T. & Bartonickova, E. Synthesis, hydration and thermal stability of hydrates in strontium-aluminate cement. *Ceram. Int.* 40, 9971–9979 (2014).
- 56. Licht, S. et al. New solar carbon capture process: STEP carbon capture. *J. Phys. Chem. Lett.* **1**, 2363–2368 (2010).
- Ekmekyapar, A., Baysar, A. & Kunkiul, A. Dehydration kinetics of Tincal and Borax by thermal analysis, Ind. *Eng. Chem. Res.* 36, 3487–3490 (1997).
- 58. Djukanovic, G. Analysis of production costs in the aluminum smelting industry. *Aluminum* 7-8 28–32 (2012).
- Kvande, H. & Drables, P. A. Aluminum smelting process and innovative alternative technologies. *JOEM* 56, S23–s31 (2014).
- Saevarsdottir, G., Kvande, H. & Welch, B. J. Aluminum production in the times of climate change: the global challenge to reduce the carbon footprint and prevent carbon leakage. JOM 72, 296–308 (2002).
- 61. Naixiang, F. et al. Towards decreasing energy consumption of aluminum reduction. *Light Met.* **2014**, 517–520 (2014).
- Granata, G., Misailidis, N., Ferreira, R., Petrides, D. Aluminum (Aluminium) production utilizing the bayer and hall-heroult process—modeling and techno-economic assessment. SuperPro Designer. https://doi.org/10.13140/RG.2.2.33228.13446 (2021).
- Aluminum. Trading Economics. https://tradingeconomics.com/ commodity/aluminum. Last accessed Aug. 19, 2024.
- The Price Trend of Cryolite Operated on a Wait-and-see Basis in May. SunSirs Commodity News. https://www.sunsirs.com/uk/detail\_ news-18601.html. Last accessed Aug. 19, 2024.
- 65. TIMESNANO. http://www.timesnano.com/en/article.php?prt=1,21. Last accessed Aug. 19, 2024.
- Licht, G., Hofstetter, K., Licht, S. Polymer composites with carbon nanotubes made from CO<sub>2</sub>. RSC Sustainability, 2, 2495–2504 (2024).
- Wang, X., Licht, G. & Licht, S. Green and scalable separation and purification of carbon materials in molten salt by efficient hightemperature press filtration. Sep. Purif. Tech. 255, 117719 (2021).
- 68. Licht, G., Hofstetter, K., Licht, S. Separation of molten electrolyte from the graphene nanocarbon product subsequent to electrolytic CO<sub>2</sub> capture, DeCarbon **4**, 100044 (2024).
- 69. Linstrom, P. J., Mallard, G. The NIST Chemistry WebBook: A Chemical Data Resource on the Internet. *J. Chem. Eng. Data*, **46** (2001).
- Malcom, J., Chase, W. NIST-JANAF thermochemical tables fourth Ed. American Chemical Society, American Institute of Physics, National Institute of Standards & Technology 1998, https://www.scribd.com/document/173465160/JPCRDM9-NIST-JANAF-Thermochemical-Tables-4th-Edition, http://webbook.nist.gov, retrieved April 22, (2024).

- Leader, M. curator, NASA Glenn ThermoBuild thermodynamic database; https://cearun.grc.nasa.gov/ThermoBuild/; last accessed April 17. (2024).
- 72. Barin, I. Thermochemical data of pure substances. Part II, ps. 1418 & 1427, VCH, Germany (1989).

#### **Acknowledgements**

We are grateful to Molood Nasirikheirabadi, Sam Mirkhani, and Amir-Reza Badri of Carbon Corp. for experimental contributions and to Emissions Reduction Alberta award IT0162473 for partial support of this research.

#### **Author contributions**

G.L. and S.L. designed the research; K.H., G.L. and S.L performed the research; S. L. and G.L. analyzed data and wrote paper.

#### Competing interests

The authors declare no competing interests.

#### **Additional information**

**Supplementary information** The online version contains supplementary material available at https://doi.org/10.1038/s42004-024-01306-z.

**Correspondence** and requests for materials should be addressed to Stuart Light.

**Peer review information** Communications Chemistry thanks Qiang Zhang and the other, anonymous, reviewers for their contribution to the peer review of this work.

Reprints and permissions information is available at http://www.nature.com/reprints

**Publisher's note** Springer Nature remains neutral with regard to jurisdictional claims in published maps and institutional affiliations.

Open Access This article is licensed under a Creative Commons Attribution 4.0 International License, which permits use, sharing, adaptation, distribution and reproduction in any medium or format, as long as you give appropriate credit to the original author(s) and the source, provide a link to the Creative Commons licence, and indicate if changes were made. The images or other third party material in this article are included in the article's Creative Commons licence, unless indicated otherwise in a credit line to the material. If material is not included in the article's Creative Commons licence and your intended use is not permitted by statutory regulation or exceeds the permitted use, you will need to obtain permission directly from the copyright holder. To view a copy of this licence, visit <a href="https://creativecommons.org/licenses/by/4.0/">https://creativecommons.org/licenses/by/4.0/</a>.

© The Author(s) 2024